Article

Developmental Cell

OsMADS6-OsMADS32 and *REP1* control palea cellular heterogeneity and morphogenesis in rice

Graphical abstract

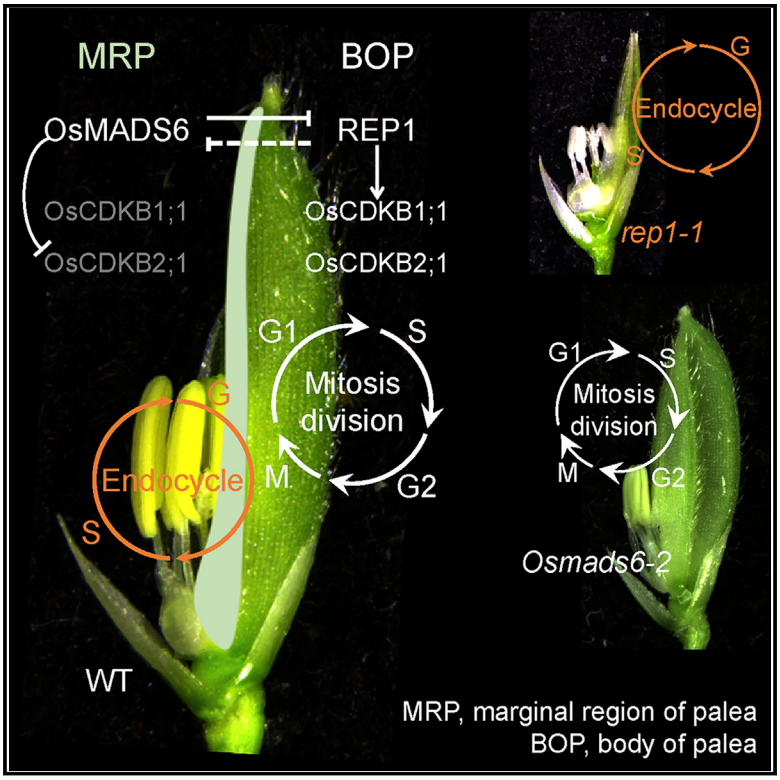

Highlights

- Rice palea exhibits distinct cellular heterogeneity during MRP and BOP development
- REP1 promotes cell division and increases palea size in BOP
- OsMADS6 and OsMADS32 modulate cell division and endoreduplication in MRP
- The OsMADS6-OsMADS32 and REP1 feedback cycle controls palea morphogenesis

Authors

Xuelian Zhang, Qiang Cai, Ling Li, ..., Dabing Zhang, Staffan Persson, Zheng Yuan

Correspondence

zyuan@sjtu.edu.cn

In brief

Zhang et al. demonstrate that mutual inhibition of OsMADS6-OsMADS32 and REP1 regulates cell cycle progression and palea morphogenesis. They highlight the significance of cellular heterogeneity in morphological diversity during organogenesis.

Zhang et al., 2024, Developmental Cell *59*, 1379–1395
June 3, 2024
https://doi.org/10.1016/j.devcel.2024.03.026

CellPress

Developmental Cell

CellPress

Article

OsMADS6-OsMADS32 and *REP1* control palea cellular heterogeneity and morphogenesis in rice

Xuelian Zhang,[1] Qiang Cai,[1,2] Ling Li,[1] Li Wang,[1] Yun Hu,[1] Xiaofei Chen,[1] Dabing Zhang,[1,3] Staffan Persson,[1,4] and Zheng Yuan[1,3,5,*]

[1]Joint International Research Laboratory of Metabolic & Developmental Sciences, State Key Laboratory of Hybrid Rice, School of Life Sciences and Biotechnology, Shanghai Jiao Tong University, Shanghai 200240, China

[2]State Key Laboratory of Hybrid Rice, College of Life Science, Wuhan University, Wuhan 430072, China

[3]Yazhou Bay Institute of Deepsea Sci-Tech, Shanghai Jiao Tong University, Sanya 572024, China

[4]Department of Plant & Environmental Sciences, Copenhagen Plant Science Center, University of Copenhagen, 1871 Frederiksberg, Denmark

[5]Lead contact

*Correspondence: zyuan@sjtu.edu.cn

https://doi.org/10.1016/j.devcel.2024.03.026

SUMMARY

Precise regulation of cell proliferation and differentiation is vital for organ morphology. Rice palea, serving as sepal, comprises two distinct regions: the marginal region (MRP) and body of palea (BOP), housing heterogeneous cell populations, which makes it an ideal system for studying organ morphogenesis. We report that the transcription factor (TF) *REP1* promotes epidermal cell proliferation and differentiation in the BOP, resulting in hard silicified protrusion cells, by regulating the cyclin-dependent kinase gene, *OsCDKB1;1*. Conversely, TFs *OsMADS6* and *OsMADS32* are expressed exclusively in the MRP, where they limit cell division rates by inhibiting *OsCDKB2;1* expression and promote endoreduplication, yielding elongated epidermal cells. Furthermore, reciprocal inhibition between the OsMADS6-OsMADS32 complex and REP1 fine-tunes the balance between cell division and differentiation during palea morphogenesis. We further show the functional conservation of these organ identity genes in heterogeneous cell growth in Arabidopsis, emphasizing a critical framework for controlling cellular heterogeneity in organ morphogenesis.

INTRODUCTION

Angiosperms, or flowering plants, exhibit diversity in flower morphology, providing a foundation for plant classification and species diversity.[1,2] This diversity is crucial for the reproductive and evolutionary success of angiosperms.[3–5] For instance, unique labellum and gynostemium innovations are linked to orchid evolution, whereas genetics underpinning peltate petal diversity underpinned evolutionary trajectories of ranunculaceous species.[6,7] Studies on model organisms such as *Arabidopsis thaliana* and *Antirrhinum majus* uncovered that angiosperm flower development, typically consisting of sepal, petal, stamen, and pistil, is regulated by a conserved ABCDE model.[8,9] Different combinations of ABCDE genes are associated with growth pattern variations and floral organ diversity. This is evident in the arrangement of non-reproductive organs, e.g., differentiated perianth with sepals and petals,[10] or diverse perianth organ formation in orchids.[11] These organs are responsible for pollinator attraction and reproductive organ protection.[12] However, how ABCDE organ identity genes regulate floral organ morphogenesis is unclear.

The flower of *Poaceae*, a monocot family, is characterized by paleas and lemmas encompassing the reproductive organs.[13,14] The term "palea" was first introduced by Carl Linnaeus in his book "Species Plantarum" in 1753.[15,16] Grasses exhibit diverse palea morphologies,[17] with Poeae spikelets usually having chartaceous paleas that are partly green.[18] Representative rice within the Poeae tribe has tough, tightly enclosed paleas and lemmas that protect reproductive organs and seeds from pathogens and insects.[19,20] Despite differences, the lemma and palea function as a bract-like structure and as sepals in eudicot florets, respectively.[19,21] The palea comprises two differentiated areas, the marginal region of the palea (MRP) and the body of the palea (BOP), that exhibit distinct cellular developments.[22] Although BOP shares lemma morphology and forms hard silicified protrusions, MRP features a transparent, smooth epidermis. The boundary between MRP and BOP radiates outward, and the palea is hooked together with the inwardly curved edge of the lemma, securely enclosing the seeds. Nevertheless, the molecular mechanism underlying cellular heterogeneity in BOP and MRP development remains poorly understood.

Morphological diversity in animals and plants arises from differential cell development,[23,24] primarily driven by cell proliferation and differentiation influenced by cell lineage and position.[25] Various factors, including morphogens,[26] mechanical stress,[27]

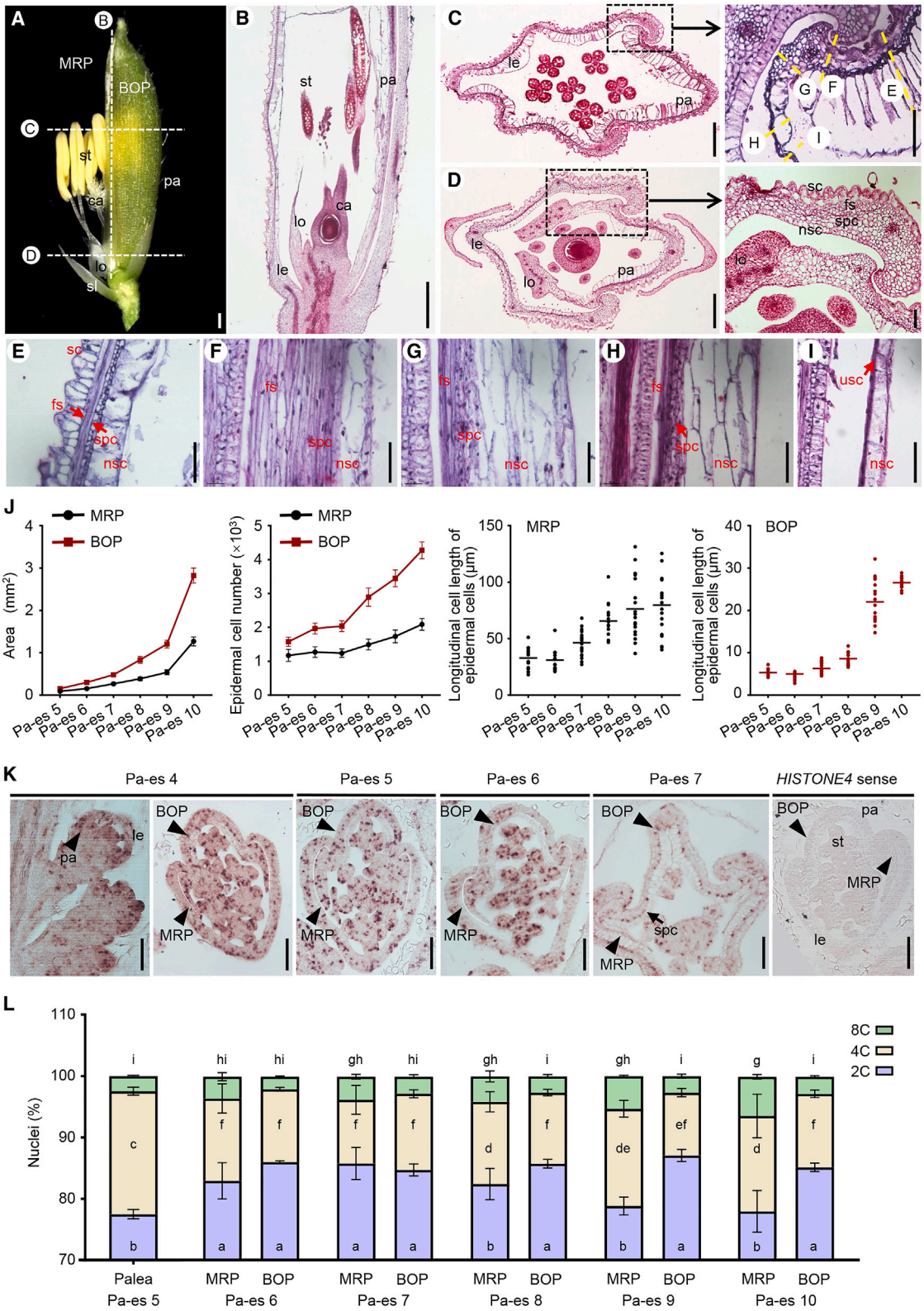

Figure 1. MRP and BOP display heterogeneous cell growth

(A) A mature wild-type (WT) rice flower is composed of a palea and lemma (removed) that enclose the internal reproductive organs. The palea consists of two distinct regions: the marginal region of palea (MRP) and the body of palea (BOP). Dashed lines show the position of the paraffin sections in (B)–(D).

(B) Longitudinal section of WT flower.

(legend continued on next page)

cell and tissue polarity,[28] and protein fluctuations, generate developmental fields to connect positional information with cell fate.[29] For example, the formation of small and giant cells in Arabidopsis sepals is attributed to fluctuating protein patterns during specific cell cycle stages.[29,30] The cell cycle progression is regulated by proteins like cyclin-dependent kinases (CDKs)/cyclin complexes.[31] In Arabidopsis, CDKA regulates the G1/S and G2/M checkpoints, while plant-specific CDKB1 and CDKB2 work as the S-G2/M-CDKs.[32,33] CDKs are protein kinases that belong to the serine-threonine family and contain a conserved aspartate (Asp, D) residue in the amino acid stretch, KLAD*FGLAR (* marks aspartate),[34] mutations of which may negatively affect the kinase activity. For instance, overexpression of Arabidopsis *CDKB1;1.N161* lines with Asp residue substitutions induces endoreduplication, leading to increased ploidy levels and epidermal cell size during the endocycle.[35,36]

In rice, *CDKB1* predominates in the late S to M stage, and *CDKB2* expression peaks in the G2 to M phase.[37,38] CDK activities are regulated by various mechanisms.[39,40] For example, lowering M-CDK activity can halt mitosis, while maintaining oscillating S-CDK activity leads to endoreduplication, resulting in chromosome doubling and increased cell size.[41] A significant increase in chromosome ploidy was observed in *OsCDKB2;1*-RNAi transgenic rice callus.[37] Meanwhile, DNA ploidy levels remained unchanged in *OsCDKB1;1*-RNAi transgenic plants, indicating different functions between OsCDKB1;1 and OsCDKB2;1 in cell cycle regulation.[42] Therefore, adjustments in cell cycle pace regulate cell size and endoreduplication, potentially driving cell heterogeneity during organ morphogenesis.

OsMADS6 and OsMADS32, belonging to the AGAMOUS LIKE 6 (AGL6) and monocot-specific MADS-box TF families, respectively, are E-function genes only expressed in *MRP*.[43–47] In *Osmads6* mutants, the palea develops a lemma-like structure, with MRP epidermal cells differentiating into silicified cells (sc). Similarly, *Osmads32* mutants display sc differentiation in part of the MRP. Conversely, RETARDED PALEA1 (REP1), a TEOSINTE BRANCHED1/CYCLOIDEA/PCF (TCP) TF family member, determines palea identity.[22] Mutations in *REP1* result in paleas with retarded growth, transparency, a smooth epidermis with five vascular bundles, and uniform epidermal cell patterns between MRP and BOP without sc differentiation. Herein, we conducted genetic and molecular analyses on *OsMADS6*, *OsMADS32*, and *REP1*, demonstrating their role in spatiotemporal regulation of cell cycle processes. This regulation contributes to heterogeneous cell division and differentiation within the rice palea epidermis and controls palea morphogenesis. Furthermore, ectopic expression of the genes in Arabidopsis identified a conserved role in regulating the cell cycle pace.

RESULTS

Palea development follows specific cell division and differentiation trajectories

To develop an integrated developmental model of rice palea, we systematically monitored cell division and differentiation patterns of the wild-type (WT) palea epidermis daily, from inflorescence primordia emergence to flowering (for details, see "STAR Methods" and Figures S1A–S1C). We employed the rice inflorescence developmental staging system as a reference.[48] The maturation of palea from primordia spans 30 days, divided into four developmental phases (A to D, Figures S1D and S1E; Table S1), further classified into twelve stages (Pa-es 0–11) based on palea epidermis cellular characteristics (Figure S1E). Phase A (Pa-es 0–1; days 0 to 12) initiates palea primordium formation as the inflorescence reaches 1.5 mm and floral organ identity begins. Phase B (Pa-es 2–4; days 13 to 17) sees inflorescence growth to 4 mm due to regular cell division and palea primordium cell expansion (Figures S1E and S1F). Phase C (Pa-es 5–10; days 18 to 22) is characterized by inflorescence growth to 54 mm and transition to asymmetrical cell differentiation along the proximal-distal and lemma-palea axes. Finally, phase D (Pa-es 11; days 23 to 30) is characterized by small, conical-shaped protrusions on epidermal cells as the inflorescence exceeds 54 mm in length (see also appendix Table S1).

During the mature stage, palea cell growth is heterogeneous along the lemma-palea axis (Figure S1C). Specifically, epidermal cells in MRP underwent differential elongation, while those in BOP were regularly shaped with protrusions. The boundary between MRP and BOP formed an interlocked hook with the lemma. We also observed heterogeneous cell growth along the proximal-distal axis, with epidermal cells displaying a basipetal growth gradient, and differentiation initiating at the distal end before other regions (Figure S1C).

MRP and BOP exhibit cellular heterogeneity

To better understand MRP and BOP cell development, we examined the cell morphology of WT palea in phase C using semithin transverse and longitudinal sections. We aimed to correlate

(C and D) Transverse sections in the middle (C), and basal (D) of the WT flower. Right insets are the enlarged parts in the squares of (C) and (D), respectively. Note that WT BOP contains four distinct cell types, which are silicified cells (sc), fibrous sclerenchyma cells (fs), spongy parenchymatous cells (spc), and non-silicified cells (nsc).

(E–I) The position of longitudinal sections from BOP to MRP are indicated by the yellow dotted lines in (C). Note that MRP lacks sc and protrusion structure (H), and the number of cell layers decreases gradually from BOP to MRP, with only two layers of cells present in the margin of MRP: undifferentiated silicified cells (usc) and nsc (I).

(J) Morphological analysis on the palea epidermis during phase C, including the area, epidermal cell number, and longitudinal epidermal cell length of MRP and BOP. Means ± SD, n > 10.

(K) *In situ* hybridization analysis of *HISTONE4* in the WT flower, showing heterogeneous cell division between MRP and BOP during palea morphogenesis. *HISTONE4* sense RNA probe was used as a control. Triangular arrowheads indicate MRP and BOP. Arrow indicates spc in BOP. BOP, body of palea; ca, carpel; fs, fibrous sclerenchyma cells; lo, lodicule; MRP, marginal region of palea; nsc, non-silicified cells; pa, palea; sc, silicified cells; sl, sterile lemma; spc, spongy parenchymatous cells; st, stamen; usc, undifferentiated silicified cells. Scale bars: 250 μm in (A) and (B), 250 μm in (C) and (D) (left), 50 μm in (C) and (D) (right), and 50 μm in (E)–(I) and (K).

(L) Distribution of nuclear ploidy in WT MRP and BOP during phase C, identifying an increase in ploidy levels in MRP compared with BOP. Means ± SD, n = 3. See also Figure S1 and Table S1.

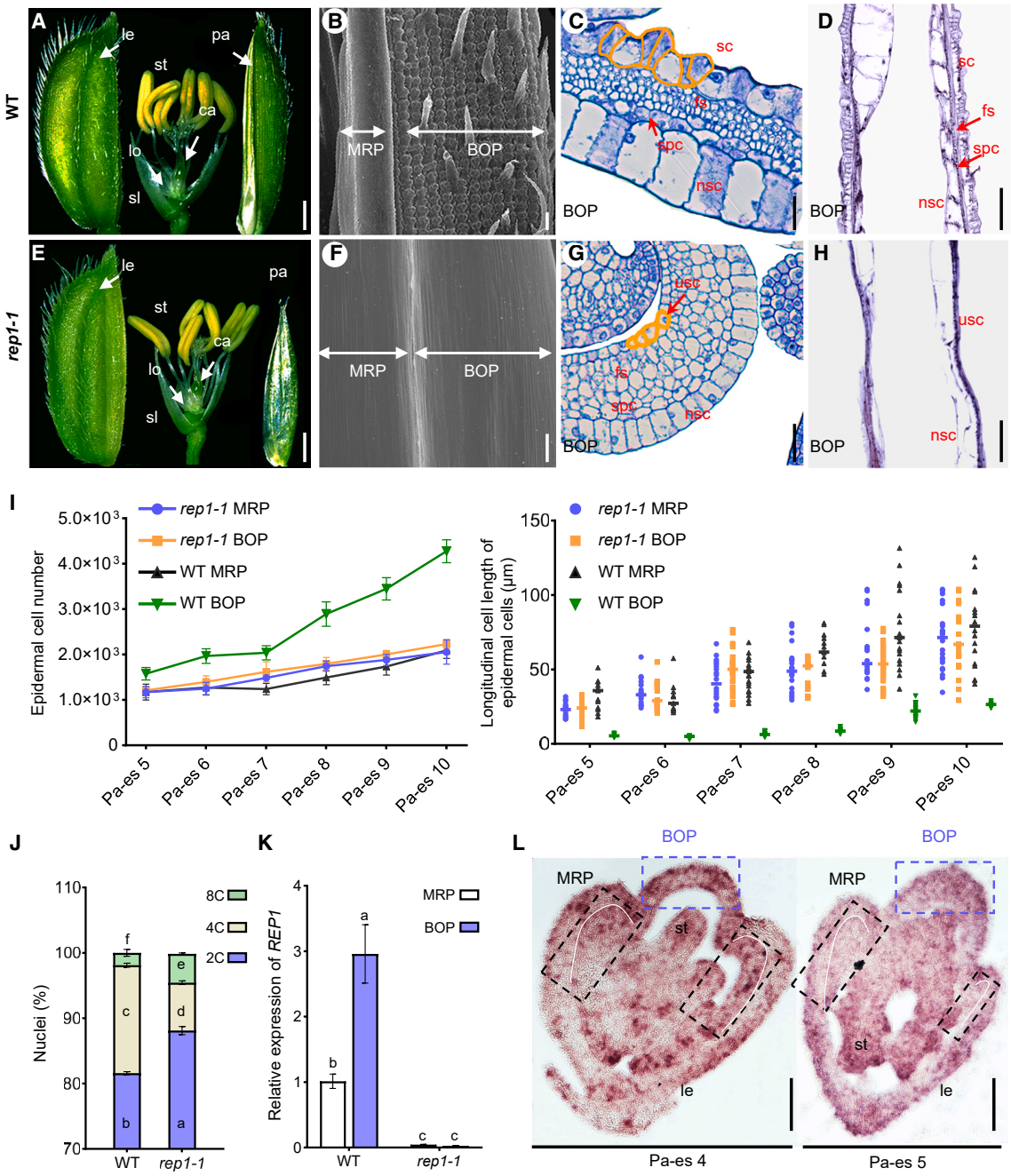

Figure 2. *REP1* promotes palea cell division and inhibits MRP epidermal cell differentiation

Cellular morphology of WT (A–D) and *rep1-1* mutant (E–H) palea.

(A and E) The WT and *rep1-1* mutant flowers, showing that *rep1-1* palea is semi-transparent with a smooth epidermis.

(B and F) Scanning electron micrograph (SEM) of WT and *rep1-1* mutant palea epidermis.

(C and G) Transverse sections of WT and *rep1-1* mutant BOP.

(D and H) Longitudinal sections of WT and *rep1-1* mutant BOP. Compared with WT, the *rep1-1* mutant palea exhibits developmental retardation, and the BOP cell division and differentiation are suppressed, leading to the loss of cellular heterogeneity between MRP and BOP and the formation of a homogeneous smooth epidermis.

(I) Statistical analysis of the WT and *rep1-1* mutant palea epidermis during phase C, including epidermal cell number and longitudinal epidermal cell length (see details in Figure S2). The epidermal cell number of BOP is reduced in *rep1-1* (left panel). The ratio of maximum to minimum lengths in *rep1-1* BOP epidermal cells increases compared with WT (right panel). Means ± SD, n > 15.

(J) Distribution of nuclear ploidy of WT and *rep1-1* mutant spikelets during phase C. The ploidy level is upregulated in the *rep1-1* mutant as compared with WT (see more information in Figure S2). Means ± SD, n = 3.

(K) Expression level of *REP1* in MRP and BOP of WT and *rep1-1* mutant. Means ± SD, n = 3. Letters indicate significant differences (one-way ANOVA: $p < 0.05$).

(legend continued on next page)

different cell types and patterns with their functions (Figures 1A–1I). The lemma cell composition remained consistent throughout the study (Figures 1C–1E). In BOP, we identified four distinct cell types from the adaxial to abaxial side: sc, fibrous sclerenchyma cells (fs), spongy parenchymatous cells (spc), and non-silicified cells (nsc). The sc displayed granular protrusions at the center of crown-shaped cells (Figure 1E), supporting and protecting the palea structure. The fs was longitudinally elongated, compressed by sc and nsc, adopting a striped shape (Figures 1E–1G). Notably, the fs nuclei became larger along the BOP-MRP axis (Figures 1F and 1G). The spc were closely packed in transverse sections (Figure 1D), with variable shapes depending on their location in longitudinal sections (Figures 1E–1H). In MRP, the spc became shorter due to expanded nsc cell volume (Figure 1H). The innermost nsc were loosely arranged and appeared as a sponge-like structure (Figures 1E–1I). Cells in the transition zone between BOP and MRP exhibited a smooth epidermis and lacked fully differentiated sc (Figures 1C, 1F, and 1G). Layers of fs and spc decreased as the transition zone approached the MRP side (Figures 1F–1H). At the edge of MRP, we only observed a densely packed layer of undifferentiated silicified cells (usc), and a less compact nsc layer (Figure 1I). Moreover, the MRP area was significantly smaller than that of BOP during phase C (Figures 1J and S1F). These observations suggest heterogeneous cell division and differentiation in MRP compared with BOP, indicating largely independent cell activities.

Epidermal growth dynamics in palea during phase C were further monitored using scanning electron microscopy (SEM). At Pa-es 5 and 6, MRP epidermal cells divided despite surface folds (Figures 1J, S1E, and S1F). From Pa-es 7 onward, MRP cells exhibited uneven lengths, some exceeding 130 μm (Figure 1J), as surface folds gradually decreased, forming smooth and undifferentiated sc. BOP epidermal cells divided both transversely and longitudinally from Pa-es 5 to 8 (Figures 1J and S1E), then rapidly elongated to a maximum length of 33 μm from Pa-es 9 onward. MRP epidermal cells exhibited diverse sizes during phase C, with a significantly lower division rate than BOP, especially between Pa-es 8 and Pa-es 9 (Figure 1J).

Changes in histone abundance and chromatin modification coincide with the cell cycle, with *HISTONE4* expression primarily observed in dividing cells.[49] To evaluate cell cycle arrest during palea development, we analyzed *HISTONE4* expression. *HISTONE4* was strongly expressed in floral meristem and throughout floral organs in Pa-es 4 and Pa-es 5 (Figure 1K). However, from Pa-es 6 onward, *HISTONE4* expression was mainly detected in BOP, particularly in intermediate fs or spc, with a gradual decline in MRP cells (Figure 1K). This indicated a gradual cell cycle arrest from MRP to BOP.

To corroborate these results, we analyzed endoreduplication levels, which stall cell division and lead to alterations in ploidy levels and increased cell size.[50] Flow cytometric analyses during phase C identified that a higher percentage of 8C cells are observed in MRP from Pa-es 8 to 10 compared with BOP (Figure 1L). There were no significant changes in the percentage of 8C cells in spikelets during phase C (Figure S1G). Thus, MRP cells exhibited an increase in ploidy levels and reduced cell division.

REP1 modulates BOP size by promoting cell division

To understand the mechanisms underlying heterogeneous cell development between MRP and BOP, we compared the shape characteristics of WT and *rep1-1* mutant. The *rep1-1* mutant exhibited stunted palea where outer epidermal cells failed to differentiate into sc, resembling MRP (Figures 2A, 2B, 2E, and 2F). The *rep1-1* mutants displayed reduced elongation in BOP, while the MRP growth rate remained unchanged compared with WT (Figures S2A–S2C), indicating that *REP1* positively regulates BOP growth.

To explore REP1's impact on BOP cell development variability, we compared epidermal and subepidermal cell morphology in WT and *rep1-1* mutants using semi-thin transverse and longitudinal sections. In *rep1-1* mutants, sc differentiation in the BOP epidermis was stalled, resulting in densely packed cells with thinner cell walls (Figures 2C and 2G). Moreover, the inner fs and spc of *rep1-1* BOP showed increased size, irregular arrangement, altered cell shape, and fewer cell layers (Figures 2D and 2H). The innermost nsc of *rep1-1* BOP exhibited significant size reduction (Figures 2C and 2G). These results indicate that *REP1* controls BOP cell development, particularly sc identity and nsc growth.

Next, we quantified epidermal cell growth dynamics during phase C in both WT and *rep1-1* mutants. *rep1-1* BOP epidermis exhibited significantly increased cell elongation compared with WT BOP (Figures 2I and S2D). Additionally, the cell division rate in *rep1-1* BOP decreased by approximately 10% compared with WT during phase C, resulting in a significant reduction in epidermal cell number (Figure 2I).

The longer epidermal cells in *rep1-1* BOP indicated a disruption in the cell cycle of *rep1-1* paleas (Figures 2I and 2J). Indeed, flow cytometry analyses identified an elevated percentage of 8C cells from Pa-es 8 to 10 during phase C for *rep1-1* (Figures S2E and S2F), with a significant increase at Pa-es 11 compared with WT (Figure 2J). Therefore, *REP1* contributes to reduced ploidy number and promotes cell division.

To investigate the *REP1* expression pattern's correlation with palea cell development, we conducted quantitative reverse-transcription PCR (RT-qPCR) and RNA *in situ* hybridization assays. We found ubiquitous *REP1* expression in MRP and BOP at Pa-es 4, with a localized increase in BOP at Pa-es 5 (Figures 2K, 2L, and S2G), supporting its role in palea development. Nonetheless, we observed no phenotypic changes in the MRP of *rep1-1* compared with WT, indicating different functions of REP1 in BOP and MRP or potential compensation by other genes in MRP.

OsMADS6 and REP1 regulate cell division differently in MRP and BOP

OsMADS6 regulates palea identity and is specifically expressed in MRP.[43,44] The *Osmads6-2* mutant exhibited reduced

(L) *In situ* RNA hybridization of *REP1* in the WT at Pa-es 4 and 5. *REP1* signals co-localize with MRP and BOP at Pa-es 4, and *REP1* signals become more pronounced in BOP at Pa-es 5. Black and purple dashed lines indicate MRP and BOP, respectively. The abbreviations correspond to those in Figure 1. Scale bars: 1 mm in (A) and (E) and 50 μm in (B)–(D), (F)–(H), and (L).
See also Figure S2.

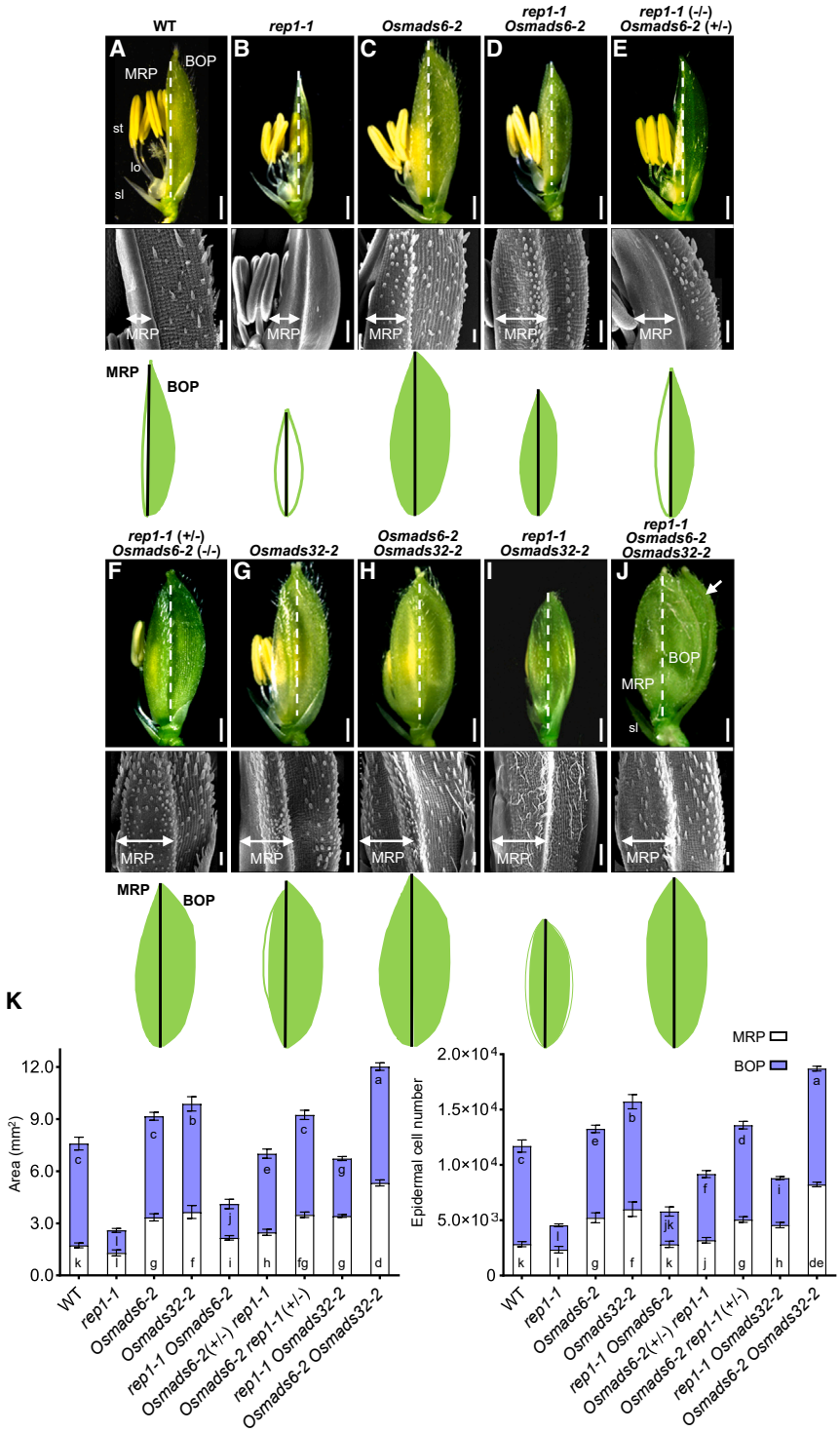

Figure 3. *OsMADS6* is epistatic to *OsMADS32* and *REP1* in inhibiting MRP epidermal cell differentiation

(A–J) Flower phenotypes (upper), SEM observation of paleas (middle), and palea diagrams (bottom) from WT, *rep1-1* single mutant, *Osmads6-2* single mutant, *rep1-1 Osmads6-2* double mutant, *rep1-1* (–/–) *Osmads6-2* (+/–) double mutant, *rep1-1* (+/–) *Osmads6-2* (–/–) double mutant, *Osmads32-2* single mutant, *Osmads6-2 Osmads32-2* double mutant, *rep1-1 Osmads32-2* double mutant, and *rep1-1 Osmads6-2 Osmads32-2* triple mutant, respectively. The palea diagrams illustrate the comparative characteristics of MRP and BOP, with the identity distinguished by a black line. The white and green filled boxes indicate a smooth MRP-like epidermis and a rough, BOP-like epidermis, respectively. Bidirectional arrows indicate MRP. Compared with WT, the retarded palea of *rep1-1* mutant displays a smooth epidermis. The enlarged palea of the *Osmads6-2* mutant exhibits epidermal protrusions. The *Osmads32-2* mutant MRP is partially transformed into a rough epidermis. Arrow in (J) indicates an extra palea-like organ. Scale bars: 1 mm in (A)–(J) (upper) and 200 μm in (A)–(J) (middle). The abbreviations correspond to those in Figure 1.

(K) Statistical analysis of palea epidermis from *rep1-1*, *Osmads6-2*, and *Osmads32-2* combinatorial mutants, including palea area (left) and epidermal cell number (right). Means ± SD, n = 10. Letters indicate significant differences (one-way ANOVA: $p < 0.05$).

See also Figure S3.

epidermal cell heterogeneity, partially suppressing palea identity (Figures 3A and 3C). *Osmads6-2* MRP showed a significant increase in size, with epidermal cells differentiated into silicified hair-like structures resembling those of the WT BOP (Figures S3A–S3D). Therefore, we used the *Osmads6-2* mutant to investigate OsMADS6's role in MRP epidermal cell growth.

Overall, longitudinal cells were significantly shorter in *Osmads6-2* MRP epidermis compared with WT MRP, leading to a narrower length range (Figures 2I and S3E). Furthermore, we found a remarkable increase (9.9%) in *Osmads6-2* MRP epidermal cell proliferation rate compared with WT during phase C, leading to more epidermal cells (Figures 3K and S3D).

Flow cytometry analyses conducted during phase C on both WT and *Osmads6-2* mutant cells determined nuclear DNA content (Figures S3G and S3H). The *Osmads6-2* mutant had increased proportions of cells in the S and G2/M phases compared with WT (Figure S3G), while there were no differences in the proportion of 8C cells (Figure S3H). These findings indicate that the *Osmads6-2* mutant drives cell division in MRP epidermal cells, impacting MRP and palea size. Furthermore, SEM analysis identified epidermal sc with distinct spiny structures and spur-like epidermal hair in the *Osmads6-2* mutant MRP (Figure 3C). OsMADS6 is, therefore, not just a regulator of epidermal cell division in MRP but also of subsequent cell differentiation.

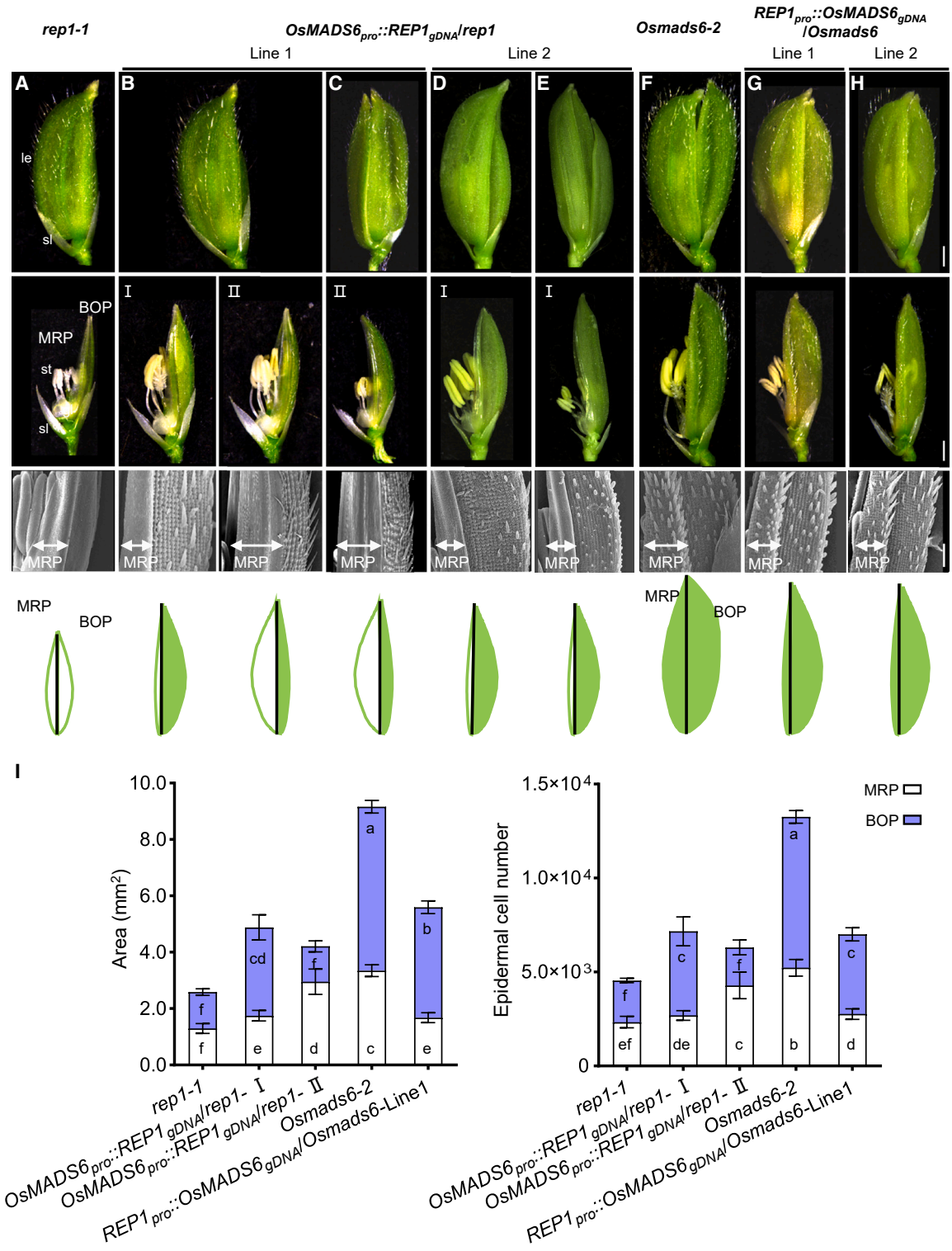

Figure 4. OsMADS6 and REP1 regulate palea development in a region-specific manner

(A–H) The sequence includes spikelet phenotypes, spikelets with lemma removed, SEM observations of paleas, and palea diagrams of *rep1-1* mutant, *OsMADS6*$_{pro}$*::REP1*$_{gDNA}$*/rep1* transgenic plant, *Osmads6-2* mutant, and *REP1*$_{pro}$*::OsMADS6*$_{gDNA}$*/Osmads6* transgenic plant, respectively. The palea diagrams illustrate the comparative characteristics of MRP and BOP, with the identity distinguished by a black line. The white and green filled boxes indicate a smooth MRP-like epidermis and a rough, BOP-like epidermis, respectively. Bidirectional arrows indicate MRP. Compared with *rep1-1*, paleas in *OsMADS6*$_{pro}$*::REP1*$_{gDNA}$*/rep1* transgenic plant displayed elongation, exhibiting various types of phenotypic recovery (type I and type II). Compared with *Osmads6-2*, paleas in

(legend continued on next page)

We next generated *Osmads6-2 rep1-1* double mutants to examine their genetic interactions in palea morphogenesis. SEM observations identified that MRP epidermal cells of the *Osmads6-2 rep1-1* double-mutant differentiate sc similarly to *Osmads6-2* single mutant (Figures 3B–3D), suggesting that *OsMADS6* is epistatic to *REP1* in regulating MRP epidermal cell differentiation. However, palea area and epidermal cell number were similar in the double-mutant and the *rep1-1* single mutant (Figure 3K), indicating that *REP1* is epistatic to *OsMADS6* in controlling palea size and cell division.

Our genetic analyses indicated a dosage effect of *OsMADS6* on palea size regulation, as evidenced by the similar palea epidermis differentiation in *rep1-1 Osmads6-2* (+/−) heterozygous double mutant and WT (Figures 3A and 3E). Additionally, the palea of the *rep1-1 Osmads6-2* (+/−) mutant was enlarged when compared with *rep1 Osmads6-2* double homozygous mutant (Figures 3D and 3E). The palea size and epidermal structure of the *rep1-1* (+/−) *Osmads6-2* mutant resembled those of *Osmads6-2* single mutant (Figures 3C, 3F, and 3K), indicating that, unlike *OsMADS6*, *REP1* does not impose a dosage-dependent regulatory effect.

OsMADS32 acts synergistically with *OsMADS6* and *REP1* in regulating cellular heterogeneity during palea development

As *OsMADS32* interacts with *OsMADS6* to regulate palea development in a dosage-dependent manner,[45] we aimed to elucidate OsMADS32's role in MRP and BOP cell heterogeneity. We observed similar differentiation of MRP sc in both *Osmads32-2* and *Osmads6-2* mutants (Figures 3C and 3G). To determine whether *OsMADS6*, *OsMADS32*, and *REP1* act synergistically to regulate palea cellular heterogeneity, we generated double and triple mutants of *Osmads6-2*, *Osmads32-2*, and *rep1-1*. SEM observations identified comparable MRP sc differentiation in the *Osmads6-2 Osmads32-2* double mutant compared with the *Osmads6-2* mutant (Figures 3C and 3H). Furthermore, the double mutant exhibited increased palea size and epidermal cell number (Figure 3K). These findings indicated that *OsMADS6* and *OsMADS32* synergistically inhibit palea cell division, with *OsMADS6* being epistatic to *OsMADS32* in MRP epidermal cell differentiation.

The palea of the *Osmads32-2 rep1-1* double mutant resembled *Osmads32-2*, except for size, akin to *rep1-1* (Figures 3G, 3I, and 3K). This indicated that *OsMADS32* is epistatic to *REP1* in MRP differentiation, akin to *OsMADS6*. However, *REP1* is epistatic to *OsMADS32* in regulating palea cell division. Interestingly, the *Osmads6-2 Osmads32-2 rep1-1* triple mutant lost palea identity, forming two palea-like organs (Figure 3J). This underscores REP1, OsMADS6, and OsMADS32's shared role in initiating palea primordia, specifying palea identity, and determining palea number.

OsMADS6 and REP1 have region-specific regulatory functions in palea development

The genetic analysis and expression patterns suggest that *OsMADS6* and *REP1* regulate palea cell development regionally. *OsMADS6* inhibits MRP cell division and differentiation, while *REP1* promotes BOP cell division and differentiation. To determine whether *OsMADS6* and *REP1* function through a common pathway in cell cycle regulation, we introduced *REP1* genomic DNA driven by the *OsMADS6* promoter into the *rep1-1* mutant and *OsMADS6* genomic DNA driven by the *REP1* promoter into the *Osmads6-2* mutant background.

Interestingly, the $OsMADS6_{pro}$::$REP1_{gDNA}$/*rep1* transgenic line displayed asymmetric MRP differentiation (Figure 4B), yielding two distinct phenotypes: type I resembling smaller WT paleas and type II resembling *rep1-1* mutant paleas (Figures 4A–4E). These results indicated that *OsMADS6* expression is essential for the outward bent hooks at the MRP-BOP junction. Moreover, about 8.5% of transgenic spikelets displayed elongated sterile lemma (Figures 4C and 4E), possibly due to *REP1* upregulation in transgenic paleas (Figure S3I). Therefore, ectopic *REP1* expression in the MRP and sterile lemma, where *OsMADS6* is specifically expressed,[51] could promote cell division and partially restore the *rep1-1* mutant phenotype.

The $REP1_{pro}$::$OsMADS6_{gDNA}$/*Osmads6* transgenic plants exhibited smaller paleas than *Osmads6-2*, particularly affecting MRP (Figures 4F–4I). Nevertheless, the overall palea epidermis morphology resembled that of *Osmads6-2*. *REP1* expression in WT paleas was lower than *OsMADS6* (Figure S3J). This suggests that the *OsMADS6* expression level in $REP1_{pro}$::$OsMADS6_{gDNA}$/*Osmads6* paleas was not sufficient to rescue the *Osmads6-2* palea epidermis phenotype (Figure S3J). Nonetheless, the chimeric construct still suppressed cell division.

OsMADS6 synergistically interacts with OsMADS32 in repressing *REP1* expression in MRP

To assess *OsMADS6*, *OsMADS32*, and REP1 expression during palea development, we conducted RT-qPCR and RNA *in situ* hybridization assays across various genotypes. REP1 expression was low but ubiquitous throughout WT palea, with prominent expression in BOP (Figures 2K, 2L, 5A, and 5B). In *Osmads6-2* palea, REP1 expression was significantly enhanced, with clear signals in MRP and BOP (Figures 5A and 5B). REP1 expression was considerably higher in *Osmads6-2 Osmads32-2* double-mutant paleas compared with *Osmads6-2* (Figure 5A). *OsMADS6* was highly expressed in WT MRP and displayed increased expression in BOP in the *rep1-1* mutant (Figures 5C and 5D). Our findings indicated that OsMADS6 and OsMADS32 collaboratively suppress REP1 expression in MRP, while REP1 inhibits *OsMADS6* expression in BOP.

To explore OsMADS6's regulation of *REP1*, we conducted chromatin immunoprecipitation-quantitative PCR (ChIP-qPCR). The *REP1* genomic region contains six CArG-box DNA motifs

$REP1_{pro}$::$OsMADS6_{gDNA}$/*Osmads6* transgenic plants become shortened, particularly in MRP. Scale bars: 1 mm in (A)–(H) (upper) and 200 μm in (A)–(H) (middle). BOP, the body of palea; lo, lodicule; MRP, the marginal region of palea; sl, sterile lemma; st, stamen.

(I) Statistical analysis of palea epidermis in *rep1-1* mutant, $OsMADS6_{pro}$::$REP1_{gDNA}$/*rep1* transgenic plant, *Osmads6-2* mutant, and $REP1_{pro}$::$OsMADS6_{gDNA}$/*Osmads6* transgenic plant, including palea area (left) and epidermal cell number (right). Means ± SD, n = 10. Letters indicate significant differences (one-way ANOVA: $p < 0.05$).

See also Figure S3.

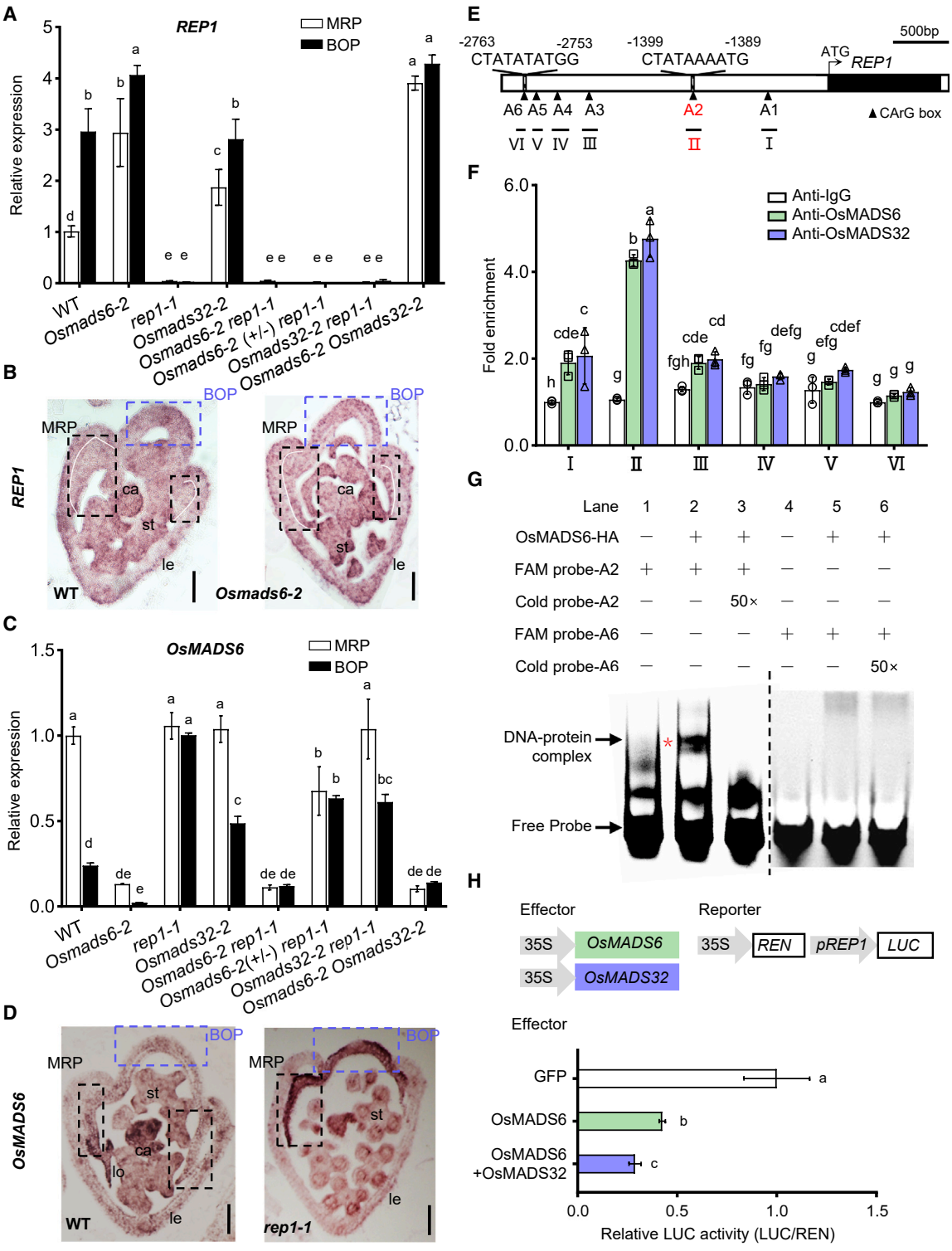

Figure 5. Mutual inhibitory effect between OsMADS6 and REP1

(A and C) Expression level of *REP1* (A) and *OsMADS6* (C) in MRP and BOP from WT, *Osmads6-2*, *rep1-1*, *Osmads32-2*, *rep1-1 Osmads6-2*, *rep1-1 Osmads6-2* (+/−), *rep1-1 Osmads32-2*, *Osmads6-2 Osmads32-2* mutants. Means ± SD, n = 3. Letters indicate significant differences (one-way ANOVA: $p < 0.05$).

(B and D) *In situ* hybridization of *REP1* (B) and *OsMADS6* (D) in the WT and the corresponding mutant palea during phase C. Black and purple dashed lines indicate MRP and BOP, respectively. Scale bars: 50 μm. The abbreviations correspond to those in Figure 1.

(E) Schematic representation of the *REP1* genomic sequence indicates six CArG-box DNA motifs [CC(A+T-rich)$_6$GG], A1–A6.

(legend continued on next page)

(A1–A6), putative binding sites for MADS proteins (Figure 5E), with OsMADS6 enriched at the A2 motif (Figures 5E and 5F). This binding was confirmed by electrophoretic mobility shift assays (EMSAs) (Figure 5G), suggesting direct binding of OsMADS6 to the *REP1* promoter. Here, luciferase reporter gene expression assays (*pREP1::LUC*) in transient tobacco leaf indicated OsMADS6's suppression of *REP1* (Figure 5H), which was enhanced when co-transformed with the OsMADS6 interactor OsMADS32 (Figure 5H),[45] and OsMADS32 also enriched at the A2 motif (Figure 5F). Consistent with the previous analysis,[45] the RT-qPCR confirmed higher *OsMADS32* expression in MRP than in BOP (Figures S4A and S4B). Hence, OsMADS6 and OsMADS32 synergistically suppress *REP1* in MRP.

By contrast, REP1, a class II TCP TF, which typically binds to GTGGNCCC or GCCCR sequences,[52] did not bind to the *OsMADS6* genomic sequence in EMSAs (Figures S3K and S3L) or show activity in dual-LUC assays with the *OsMADS6* promoter (*pOsMADS6::LUC*) in tobacco leaves (Figure S3M), suggesting indirect suppression of *OsMADS6* in BOP.

Cell cycle processes are induced in the palea of *rep1-1*, *Osmads6-2*, and *Osmads32-2* mutants

To investigate what molecular pathways that *OsMADS6*, *OsMADS32*, and *REP1* impact, we undertook RNA-Sequencing analysis (RNA-Seq) on phase C palea samples from WT, *rep1-1*, *Osmads6-2*, and *Osmads32-2* mutants (Figure S4C). In total, we identified significant changes ($|\text{fold change}| > 2$; $P < 0.01$) in the expression of 3,189, 3,597, and 1,543 genes in *rep1-1*, *Osmads6-2*, and *Osmads32-2* mutants, respectively, compared with WT (Figures S4C–S4E). We verified selected genes using RT-qPCR on an independent set of palea samples from WT, *rep1-1*, *Osmads6-1*, and *Osmads32-2* mutants (Figure S4F).

Since MRP and BOP exhibit heterogeneous cell development, differentially expressed genes (DEGs) associated with the cell cycle were investigated in the *rep1-1*, *Osmads6-1*, and *Osmads32-2* mutants. Among them, 18 DEGs were obviously downregulated in the *rep1-1* mutant (Figures S4D and S4E), whereas 15 DEGs related to DNA replication, cell cycle, and cell proliferation were upregulated in the *Osmads6-2* and *Osmads32-2* mutants (Figures S4D and S4E). In total, we screened 11 putative downstream cell cycle genes regulated by REP1, OsMADS6, or OsMADS32 based on their expression pattern (Figure S4D; Table S2).

The *Osmads6-2* mutant showed accelerated cell division, with increased cells in DNA replication and mitotic phases compared with WT palea (Figures S3G and S3H). Conversely, the *rep1-1* mutant exhibited high endoreduplication, leading to a rise in 8C cell counts and reduced cell proliferation compared with WT (Figure S2E). These observations indicated that OsMADS6 may upregulate cell cycle inhibitors or suppress cell cycle-promoting factors, while REP1 might promote cell cycle-promoting factors or suppress cell cycle inhibitors. Bioinformatic inferences and luciferase assays indicated potential targets as *OsCDKB2;1* (OsMADS6 regulated) and *OsCDKB1;1* (REP1 regulated) (Table S2).

OsMADS6 represses *OsCDKB2;1* expression to suppress cell division in MRP

To corroborate *OsCDKB2;1* regulation by OsMADS6, we performed RNA *in situ* hybridization and RT-qPCR. *OsCDKB2;1* transcript were mainly detected in WT palea, with higher expression in BOP than in MRP (Figures 6A and 6B). However, in *Osmads6-2*, *OsCDKB2;1* expression expanded throughout the subepidermal cell layers of MRP (Figure 6A), accompanied by significant upregulation (Figure 6B). Hence, we postulated that OsMADS6 inhibits *OsCDKB2;1* expression in MRP. Our ChIP-qPCR identified enrichment of both OsMAD6 and OsMADS32 in two potential regulatory regions (I and II) of the *OsCDKB2;1* promoter, containing three CArG-box DNA motifs (E1–E3) (Figures 6C and 6D). Moreover, EMSA analysis identified that OsMADS6 is specifically bound to E1 and E2 probes (Figure 6E). Dual-LUC assays in tobacco leaves confirmed that OsMADS6 could repress *OsCDKB2;1* expression (*pOsCDKB2;1::LUC*). Nevertheless, co-transformation with OsMADS32 did not significantly alter this suppression (Figure 6F).

We conducted experiments to elucidate OsMADS6's genetic regulation of *OsCDKB2;1*. CRISPR-Cas9 mutagenesis targeted the 5′ UTR and catalytic domain of *OsCDKB2;1*, yielding two knockout alleles (Figure S5A). The *OsCDKB2;1* mutants did not show any obvious palea phenotype compared with WT (Figure S5B). Therefore, we overexpressed a dominant-negative allele of *OsCDKB2;1* (*OX-CDKB2;1D-N*), which negatively affects kinase activity,[35,53] in both WT and *Osmads6-2* backgrounds (Figures 6G and S5B–S5E). Although *OX-CDKB2;1D-N*/WT plants showed no apparent palea phenotype (Figures S5C–S5E), *OX-CDKB2;1D-N*/*Osmads6* plants had shortened paleas with narrower MRP compared with *Osmads6-2* (Figure 6G). Additionally, *OX-CDKB2;1D-N*/*Osmads6* plants showed reduced palea size and epidermal cell count (Figure 6H). Flow cytometric analyses at Pa-es 11 identified a higher percentage of 8C cells in *OX-CDKB2;1D-N*/*Osmads6* spikelets compared with *Osmads6-2* (Figure 6I). These findings underscore the critical role of the OsMADS6-OsCDKB2;1 regulatory module in palea development, particularly in MRP cell division.

REP1 activates *OsCDKB1;1* expression to promote cell division in palea

To understand REP1's molecular regulation of *OsCDKB1;1*, we employed RNA *in situ* hybridization, observing *OsCDKB1;1*

(F) Chromatin immunoprecipitation-quantitative polymerase chain reaction (ChIP-qPCR) results for the six targeted amplicons, regions I to VI. OsMADS6 and OsMADS32 specifically bind to region II of the *REP1* promoter. Enrichment was compared with the input sample. Mean ± SD, n = 3.
(G) Electrophoretic mobility-shift assay (EMSA) using the OsMADS6 proteins and fragments of the *REP1* promoter containing CArG-box DNA motifs (A2 and A6) as probes labeled with 5′-FAM. OsMADS6 binds to the A2 motif of the *REP1* promoter. A 50× excess of nonlabeled probes was used for competition. Asterisk indicates the DNA-protein complex.
(H) Transient dual-luciferase (LUC) assays showed that OsMADS32 enhances the transcriptional repression of OsMADS6 on *REP1*. Constructs are shown in the upper panel; the *REP1* promoter in the reporter construct contains a promoter sequence upstream of the start codon. Means ± SD, n = 6.
See also Figure S3.

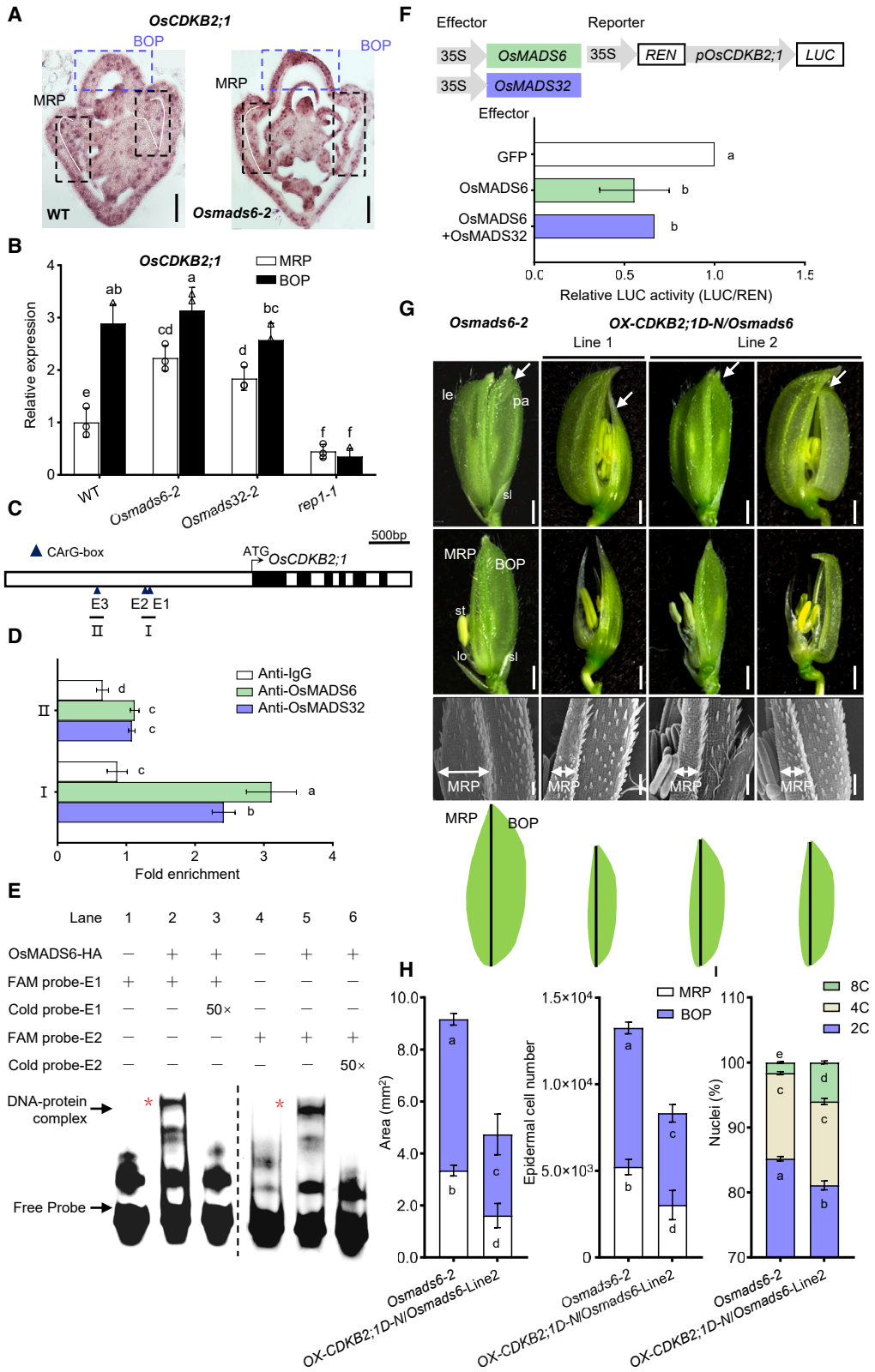

Figure 6. OsMADS6 directly represses the expression of *OsCDKB2;1* to regulate MRP development

(A) *In situ* hybridization of *OsCDKB2;1* in the WT and *Osmads6-2* mutant palea. Black and purple dashed lines indicate MRP and BOP, respectively. Scale bars: 50 μm.

(legend continued on next page)

expression in BOP sc and punctate signals at MRP edge in WT, whereas it became more dispersed in *rep1-1* mutant palea (Figure S6A). RT-qPCR confirmed reduced *OsCDKB1;1* expression in *rep1-1* MRP and BOP (Figure S6B), indicating REP1 enhances *OsCDKB1;1* expression. EMSA identified that REP1 specifically bind to the F1 and F2 sites, TCP TF binding sites in the *OsCDKB1;1* genomic region (Figures S6C and S6D). Dual-LUC assays in tobacco leaves identified that REP1 could specifically bind to the *OsCDKB1;1* promoter and induce LUC expression (*pOsCDKB1;1::LUC*) (Figure S6E).

To further explore REP1's regulatory role on *OsCDKB1;1*, we conducted genetic analyses. We generated *OX-CDKB1;1*/WT and *OX-CDKB1;1/rep1-1* plants by over-expressing *OsCDKB1;1* in WT and *rep1-1* mutant, respectively (Figures S6F–S6J). *OX-CDKB1;1*/WT plants displayed WT floral organ phenotypes (Figures S6G and S6J). However, *OsCDKB1;1* overexpression in *rep1-1* mutant rescued the growth retardation phenotype of paleas by promoting BOP epidermal cell differentiation into sc and subsequent trichome formation (Figures S6G–S6J). Approximately 20.4% of transgenic spikelets showed enlarged paleas with well-differentiated MRP and BOP structures akin to *Osmads6-2* (Figure S6J). Furthermore, *OX-OsCDKB1;1/rep1* plants showed significantly increased palea size and epidermal cell number (Figures S6G and S6H). Flow cytometric analysis at Pa-es 11 identified a reduced percentage of 8C cells in *OX-OsCDKB1;1/rep1* spikelets compared with *rep1-1* (Figure S6I). These findings indicated that a regulatory module of REP1-OsCDKB1;1 plays a significant role in palea development, particularly in controlling cell division of BOP.

REP1, *OsMADS6*, and *OsMADS632* regulatory roles in cellular heterogeneity are conserved in Arabidopsis

To assess the conservation of cell cycle regulatory functions of *OsMADS6*, *OsMADS32*, and *REP1* across species, their open reading frames (ORFs) were placed under a constitutive 35S promoter and introduced into *Arabidopsis thaliana* (Figures 7A and S7A). *REP1* over-expressing plants displayed Columbia-0 (Col-0)-like phenotypes (Figure 7A), while Arabidopsis plants expressing *OsMADS6* exhibited stunted growth, reduced rosette leaves, shorter petioles, and early flowering (Figure 7A). Similarly, *OsMADS32*-expressing Arabidopsis plants displayed stunted growth, fewer rosette leaves, altered leaf shapes, and shorter petioles (Figure 7A). Moreover, cellular growth analyses showed that *35S::OsMADS6* and *35S::OsMADS32* seedlings had reduced total leaf area and reduced epidermal cell number in the second leaf compared with Col-0 and *35S::REP1* (Figures S7B and S7C).

WT and the transgenic Arabidopsis seedlings were analyzed using flow cytometry to investigate the effects of *OsMADS6*, *REP1*, and *OsMADS32* on cell cycle and leaf cell growth. At 18 days after germination (DAG), the proportion of 2C and 4C cells was 53.0% ± 3.1% in WT, whereas it increased to 60.1% ± 1.2% in *35S::REP1* seedlings (Figure S7D), indicating that REP1 promotes cell division. The percentage of 2C and 4C cells was 83.9% ± 1.0% in *35S::OsMADS6* seedlings, with a decrease in polyploid cells (such as 8C and 16C) compared with WT. Here, leaf epidermal cells were reduced in size leading to an increased cell density, with a few cells elongated along the proximal-distal axis (Figure S7E), indicating that *OsMADS6* induces cell division in Arabidopsis leaf cells. Conversely, the percentage of 2C and 4C cells in *35S::OsMADS32* seedlings was reduced to 39.6% ± 0.2%, while the number of polyploid cells increased (Figure S7D). Small cells were abnormally clustered around guard cells in *35S::OsMADS32* leaves, and epidermal cells elongated along the mid-lateral axis (Figure S7E), indicating that OsMADS32 induces endoreduplication of Arabidopsis leaf cells.

OsMADS6, OsMADS32, and REP1 are regulatory factors in rice floral organ development, particularly the palea, which exhibits homology with the sepal of Arabidopsis. We examined reproductive phenotypes in over-expressing plants (Figure 7A), noting significant changes in perianth development. Petals and sepals of *35S::OsMADS6* and *35S::OsMADS32* were smaller than those of WT (Figure S7B), while those of *35S::REP1* were slightly larger (Figures 7A and S7B).

To investigate if perianth size changes in over-expressing plants affect cell behavior, we analyzed giant cell numbers in the adaxial epidermal layer of mature sepals. In *35S::OsMADS32* sepals, the proportion of highly endoreduplicated epidermal nuclei increased (Figures 7A and S7F), whereas *35S::OsMADS6* showed a lower proportion of endoreduplicated giant cells compared with the WT and *35S::REP1* (Figures 7A and S7F). This suggests *OsMADS32* promotes sepal size partly by enhancing cell endoreduplication. Similarly, *OsMADS6* overexpression inhibited endoreduplication and stimulated cell

(B) Expression level of *OsCDKB2;1* in MRP and BOP of WT, *Osmads6-2*, *rep1-1*, and *Osmads32-2* mutants, respectively. Means ± SD, n = 3.
(C) Schematic representation of the *OsCDKB2;1* genomic sequence showing three CArG-box DNA motifs [CC(A+T-rich)$_6$GG], E1–E3.
(D) ChIP-qPCR results for the two targeted amplicons, regions I (including E1 and E2) and II. OsMADS6 and OsMADS32 bind to region I of *OsCDKB2;1* promoter. Enrichment was compared with the input sample. Mean ± SD, n = 3.
(E) EMSA using the OsMADS6 proteins and fragments of the *OsCDKB2;1* promoter containing CArG-box DNA motifs as probes labeled with 5′-FAM. OsMADS6 specifically binds to E1 and E2. A 50× excess of nonlabeled probes was used for competition. Asterisk indicates the DNA-protein complex.
(F) LUC assays to show OsMADS6 binding to the *OsCDKB2;1* promoter to repress its expression. Constructs are shown in the upper panel. Means ± SD, n = 6.
(G) The sequence includes spikelet phenotypes, spikelets with lemma removed, SEM observations of paleas, and palea diagrams of *Osmads6-2* mutant and *OsCDKB2;1D-N/Osmads6* transgenic lines, respectively. The palea diagrams illustrate the comparative characteristics of MRP and BOP, with the identity distinguished by a black line. The white and green filled boxes indicate a smooth MRP-like epidermis and a rough, BOP-like epidermis, respectively. Bidirectional arrows indicate MRP. Compared with *Osmads6-2*, paleas in *OsCDKB2;1D-N/Osmads6* transgenic plant exhibited shortening, particularly in MRP. Scale bars: 1 mm (upper) and 200 μm (middle). The abbreviations correspond to those in Figure 1.
(H) Statistical analysis of palea epidermis in *Osmads6-2* mutant and *OsCDKB2;1D-N/Osmads6*-Line2 transgenic lines, including palea area (left) and epidermal cell number (right). Means ± SD, n = 10. Letters indicate significant differences (one-way ANOVA: $p < 0.05$).
(I) Distribution of nuclear ploidy in *Osmads6-2* and *OsCDKB2;1D-N/Osmads6*-Line2 spikelets at Pa-es 11. The ploidy level increased in *OsCDKB2;1D-N/Osmads6*-Line2 when compared with *Osmads6-2*. Means ± SD, n = 3.
See also Figures S4, S5 and S6 and Table S2.

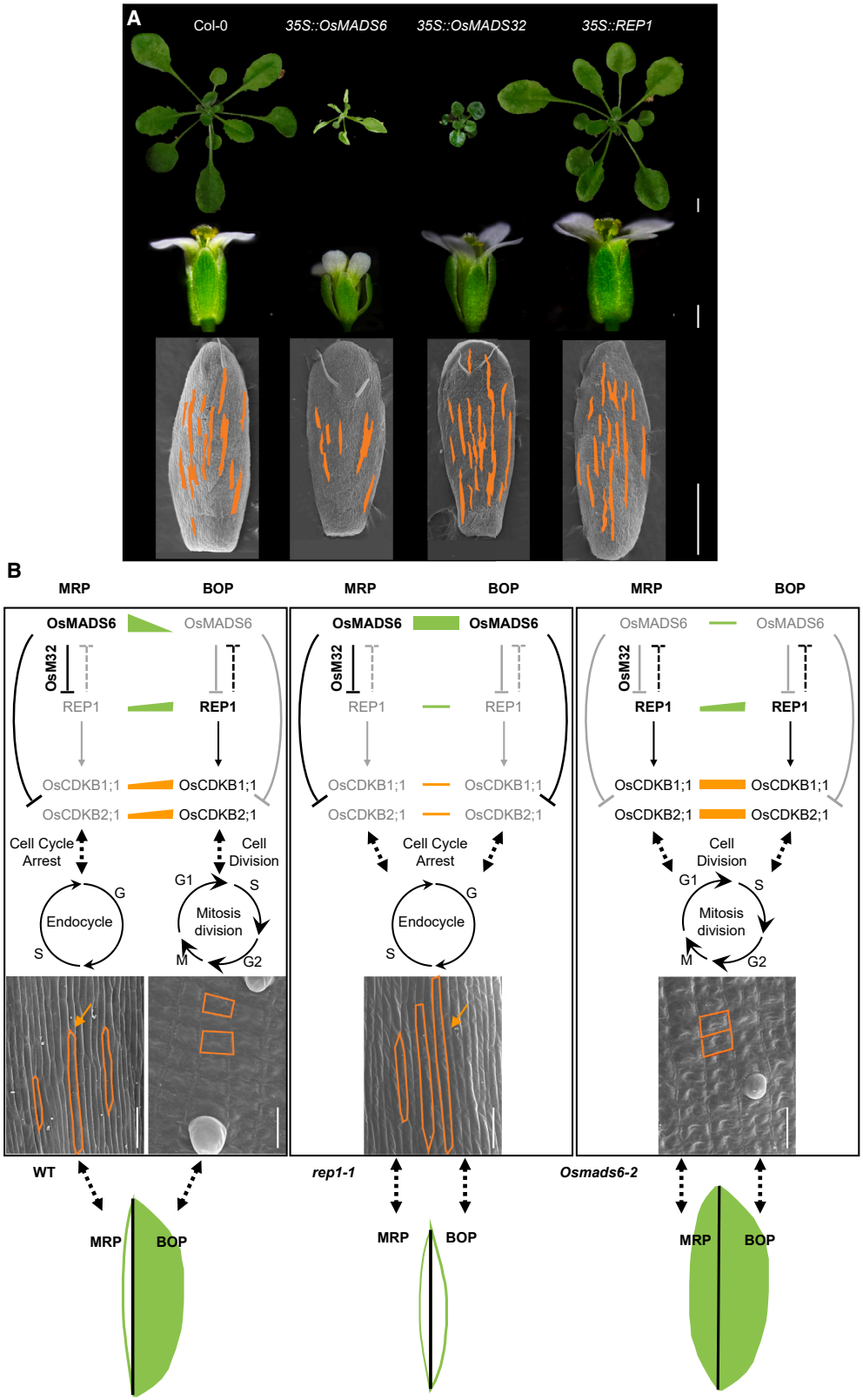

Figure 7. Hypothetical model of OsMADS6, OsMADS32, and REP1 in regulating cell growth heterogeneity in rice palea

(A) Effects of ectopic expressions of *OsMADS6*, *OsMADS32*, and *REP1* on Arabidopsis vegetative growth (18 DAG), flowers from side view, and sepals (giant cells are marked in orange). Scale bars: 500 μm.

(legend continued on next page)

division in Arabidopsis sepals, as observed in paleas. In mature petals, *35S::REP1* had more epidermal cells than WT (Figure S7C), while *35S::OsMADS32* and *35S::OsMADS6* had fewer (Figure S7C). These results suggest that *OsMADS6*, *REP1*, and *OsMADS32* play crucial roles in cell cycle regulation across plant species.

DISCUSSION

Grasses display considerable variations in floral morphology that correlate with their evolutionary past.[55,56] In this context, the palea is of particular interest due to its plasticity and heterogeneity. The palea is a thin and fragile structure enclosed by glumes in wheat,[57] it degenerates in the maize ear (female) and is membranous in the maize tassel (male).[19,58] By contrast, rice features a distinctive palea structure that safeguards reproductive organs and seeds during development. Our findings demonstrate that a mutually inhibitory framework controls cell heterogeneity during palea morphogenesis.

Heterogeneous cell growth is essential for robust organ and tissue formation in eukaryotic organisms.[23,59,60] For instance, barley palea exhibits heterogeneous cell growth, where the central region has thickened cell walls that hinder cell expansion,[61] but the molecular mechanisms underlying such heterogeneity are unclear. We outline how TFs *REP1*, *OsMADS6*, and *OsMADS32* regulate cell cycle progression in palea tissues to control morphogenesis (Figure 7B). Similar regulatory roles of MADS-box and TCP TFs have been observed in *Senecio vulgaris*, *Phalaenopsis equestris*, *Aristolochia fimbriata*, tomato, Arabidopsis, and bryophytes,[62–65] depending on their expression patterns. We show how controlled expression of *OsMADS6* and *OsMADS32* in MRP promotes heterogeneous epidermal cell growth. These TFs and *REP1* alter *OsCDKB1;1* and *OsCDKB2;1* expression, which impacts BOP and MRP cell proliferation and differentiation. Reduced *OsCDKB1;1* and *OsCDKB2;1* expression slows MRP cell division while promoting endoreduplication. This regulation then drives the differential morphology of MRP and BOP (Figure 7B). Hence, understanding the interplay of *OsMADSs* and *REP1* in different palea regions contributes to our knowledge of grass evolution and domestication.

The balance between cell division and differentiation is crucial in determining organ growth and morphological stability in Arabidopsis.[66] Although certain aspects of *OsMADS6*, *OsMADS32*, and *REP1* appear to be conserved between rice and Arabidopsis, the function of *OsMADS6* may vary. Although *OsMADS6* inhibits cell division in MRP, it stimulates cell division in Arabidopsis leaves and sepals (Figure 7A). This difference could stem from evolutionary changes in MADS TF function or that OsMADS6 does not function properly in the Arabidopsis context. Previous studies identified that class II TCP TFs, like *CYCLOIDEA* (*CYC*) in snapdragons,[67,68] and *COMPOSITUM1* (*COM1*) in barley suppress cell proliferation and influence perianth development.[61] By contrast, related TFs *BdWAB1/BAD1* in Brachypodium and *SbWAB1/BAD1* in Sorghum have no effect on perianth development.[61] Nevertheless, our research showed that *REP1* supports cell division in Arabidopsis leaves, sepals, and rice paleas (Figures 2E and 7A).

Our analysis of palea morphology in *rep1-1*, *Osmads6-2* (+/−) *rep1-1*, *Osmads6-2 rep1-1* combinatorial mutants, and $REP1_{pro}$::$OsMADS6_{gDNA}$/*Osmads6* transgenic lines confirmed the gene dosage effect of *OsMADS6* on palea morphogenesis. This indicates that OsMADS6 regulates palea development by reaching a certain threshold, triggering a transition between mitosis and endoreduplication. Therefore, investigating the spatiotemporal levels of the OsMADS6 protein along the lemma-palea axis during palea morphogenesis and its regulatory mechanisms is warranted.

The *Osmads6-2 Osmads32-2 rep1-1* triple mutant produced two palea-like structures in its flower, confirming the importance of OsMADS6, OsMADS32, and REP1 in specifying palea identity and numbers.[44,45] Monocot flowers typically have trimerous arrangements of floral organs.[4,69] However, the regulatory mechanisms and evolutionary processes that govern the number and position of these organs are not fully understood. Multiple mechanisms, including boundary formation and primordia fusion, determine the quantity and position of floral organs.[69,70] The increased palea number in the triple mutant may result from anomalies in primordia boundaries or fusion. The precise regulation of palea identity and optimal quantity in *Poaceae* is crucial for functional specialization during evolution. Mathematical models may aid in understanding mechanisms governing palea development and perhaps explain the significance of palea number in rice and grass evolution. In summary, our findings outline a mechanism that underpins flower organ morphogenesis and identify that plants may use organ identity genes and cell cycle regulators to control cellular heterogeneity to produce varied morphologies.

Limitations of the study

Our data demonstrate that the mutual inhibition between the OsMADS6-OsMADS32 complex and REP1 coordinates the variation in cell types during palea morphogenesis. Future studies that examine the spatiotemporal levels of these proteins will

(B) The rice palea comprises two distinct regions, MRP and BOP, displaying heterogeneity in cellular composition and behavior. In the BOP, REP1 facilitates S-CDK *OsCDKB1;1* expression while repressing *OsMADS6* to allow M-CDK *OsCDKB2;1* expression. Elevated OsCDKB1;1 and OsCDKB2;1 levels promote normal proliferation and epidermal cell differentiation, forming a silicified enlarged BOP. In the MRP, OsMADS6, and OsMADS32 inhibit *REP1* and M-CDK *OsCDKB2;1* expression, reducing *OsCDKB1;1* and *OsCDKB2;1* levels, thus decreasing the division rate and promoting epidermal cell elongation through endoreduplication. In the *rep1-1* mutant BOP, *OsCDKB1;1* is downregulated while *OsMADS6* is upregulated, leading to *OsCDKB2;1* downregulation and subsequent epidermal cell endoreduplication, resembling MRP cell patterns. Conversely, the MRP of *Osmads6-2* mutant upregulates *OsCDKB2;1* and *REP1*, increasing *OsCDKB1;1* expression and promoting cell division and differentiation, resembling BOP cells.

The expression patterns of *OsMADS6* and *REP1* are illustrated in green, while those of *OsCDKB1;1* and *OsCDKB2;1* are shown in orange. Cell boundaries are shown using orange circles. MRP and BOP are represented by unfilled and filled green boxes, respectively, with the boundary between them marked by a black line. Schematic diagrams for cell cycle and endoreduplication were adapted from Lang and Schnittger.[54] BOP, body of palea; G1, the Gap 1 phase; G2, the Gap 2 phase; M, the mitosis phase; MRP, marginal region of palea; S, the synthesis phase; WT, wild type.

See also Figure S7.

shed light on their specific roles in this process and might address when and how these TFs were recruited during the evolution and domestication of grasses.

STAR★METHODS

Detailed methods are provided in the online version of this paper and include the following:

- KEY RESOURCES TABLE
- RESOURCE AVAILABILITY
  - Lead contact
  - Materials availability
  - Data and code availability
- EXPERIMENTAL MODEL AND STUDY PARTICIPANT DETAILS
  - Plant materials and growth conditions
- METHOD DETAILS
  - Constructs and plant transformation
  - Histological analysis and microscopy observation
  - Flow cytometry analysis
  - Quantitative reverse-transcription PCR assays
  - *In situ* hybridization
  - Dual-luciferase assay
  - ChIP-qPCR
  - Electrophoretic mobility-shift (EMSA) assays
  - RNA-Sequencing (RNA-Seq) and analysis
  - Accession numbers
- QUANTIFICATION AND STATISTICAL ANALYSIS
  - Statistical analysis

SUPPLEMENTAL INFORMATION

Supplemental information can be found online at https://doi.org/10.1016/j.devcel.2024.03.026.

ACKNOWLEDGMENTS

We would like to express our gratitude to Mr. Zhijing Luo, Ms. Mingjiao Chen, and Mr. Ting Luo for their assistance in rice cultivation; Mr. Liang Zhang and Mr. Baozhe Ping for their contribution in collecting RNA-seq samples and executing paraffin sections; Prof. Dexing Xiao for paraffin sections; Prof. Xinguang Zhu (SIPPE, CAS) and Ms. Yanxia Mai (Core Facility Center of CEPMS/SIPPE, CAS) for the support on the flow cytometer analysis; the Core Facility and Service Center (CFSC) for School of Life Sciences and Biotechnology, and SJTU for the support on the SEM data collection. This work was supported by grants from the National Key Research and Development Program of China (2022YFD1200102); the National Natural Science Foundation of China (32170322 and 31671260); Special Funds for Construction of Innovative Provinces in Hunan Province (2021NK1002); the Sino-Germany Mobility Program (M-0141); China Innovative Research Team, Ministry of Education, and the Programme of Introducing Talents of Discipline to Universities (111 Project, B14016); and the SMC Morningstar Young Scholarship of Shanghai Jiao Tong University to Z.Y.. S.P. acknowledges the financial aid of Villum Investigator (project ID: 25915), DNRF Chair (DNRF155), Novo Nordisk Laureate (NNF19OC0056076), Novo Nordisk Emerging Investigator (NNF20OC0060564), Novo Nordisk Data Science (NNF0068884), and Lundbeck Foundation (experiment grant, R346-2020-1546) grants.

AUTHOR CONTRIBUTIONS

Conceptualization, Z.Y.; methodology, X.Z., Q.C., L.W., L.L., Y.H., and X.C.; investigation, X.Z., and Z.Y.; writing-original draft, review, and editing, X.Z., S.P., and Z.Y.; supervision, S.P., D.Z., and Z.Y.; funding acquisition, D.Z. and Z.Y.

DECLARATION OF INTERESTS

The authors declare no competing interests.

Received: June 20, 2023
Revised: January 2, 2024
Accepted: March 12, 2024
Published: April 8, 2024

REFERENCES

1. Endress, P.K. (2011). Evolutionary diversification of the flowers in angiosperms. Am. J. Bot. *98*, 370–396. https://doi.org/10.3732/ajb.1000299.
2. Armbruster, W.S. (2014). Floral specialization and angiosperm diversity: phenotypic divergence, fitness trade-offs and realized pollination accuracy. AoB Plants *6*, plu003. https://doi.org/10.1093/aobpla/plu003.
3. Sauquet, H., and Magallón, S. (2018). Key questions and challenges in angiosperm macroevolution. New Phytol. *219*, 1170–1187. https://doi.org/10.1111/nph.15104.
4. Smyth, D.R. (2018). Evolution and genetic control of the floral ground plan. New Phytol. *220*, 70–86. https://doi.org/10.1111/nph.15282.
5. Sauquet, H., von Balthazar, M., Magallón, S., Doyle, J.A., Endress, P.K., Bailes, E.J., Barroso de Morais, E., Bull-Hereñu, K., Carrive, L., Chartier, M., et al. (2017). The ancestral flower of angiosperms and its early diversification. Nat. Commun. *8*, 16047. https://doi.org/10.1038/ncomms16047.
6. Cheng, J., Yao, X., Li, X., Yue, L., Duan, X., Li, B., Fu, X., Li, S., Shan, H., Yin, X., et al. (2023). Diversification of ranunculaceous petals in shape supports a generalized model for plant lateral organ morphogenesis and evolution. Sci. Adv. *9*, eadf8049. https://doi.org/10.1126/sciadv.adf8049.
7. Zhang, G.-Q., Liu, K.-W., Li, Z., Lohaus, R., Hsiao, Y.-Y., Niu, S.-C., Wang, J.-Y., Lin, Y.-C., Xu, Q., Chen, L.-J., et al. (2017). The Apostasia genome and the evolution of orchids. Nature *549*, 379–383. https://doi.org/10.1038/nature23897.
8. Theissen, G., and Saedler, H. (2001). Plant biology. Floral quartets. Nature *409*, 469–471. https://doi.org/10.1038/35054172.
9. Theißen, G., Melzer, R., and Rümpler, F. (2016). MADS-domain transcription factors and the floral quartet model of flower development: linking plant development and evolution. Development *143*, 3259–3271. https://doi.org/10.1242/dev.134080.
10. Monniaux, M., and Vandenbussche, M. (2018). How to Evolve a Perianth: A Review of Cadastral Mechanisms for Perianth Identity. Front. Plant Sci. *9*, 1573. https://doi.org/10.3389/fpls.2018.01573.
11. Hsu, H.-F., Hsu, W.-H., Lee, Y.-I., Mao, W.-T., Yang, J.-Y., Li, J.-Y., and Yang, C.-H. (2015). Model for perianth formation in orchids. Nat. Plants *1*, 15046. https://doi.org/10.1038/nplants.2015.46.
12. Warner, K.A., Rudall, P.J., and Frohlich, M.W. (2009). Environmental control of sepalness and petalness in perianth organs of waterlilies: a new Mosaic theory for the evolutionary origin of a differentiated perianth. J. Exp. Bot. *60*, 3559–3574. https://doi.org/10.1093/jxb/erp202.
13. Schmidt, R.J., and Ambrose, B.A. (1998). The blooming of grass flower development. Curr. Opin. Plant Biol. *1*, 60–67. https://doi.org/10.1016/s1369-5266(98)80129-5.
14. Callens, C., Tucker, M.R., Zhang, D., and Wilson, Z.A. (2018). Dissecting the role of MADS-box genes in monocot floral development and diversity. J. Exp. Bot. *69*, 2435–2459. https://doi.org/10.1093/jxb/ery086.
15. von Linné, C., and Salvius, L. (1753). Caroli Linnaei ... Species plantarum:exhibentes plantas rite cognitas, ad genera relatas, cum differentiis specificis, nominibus trivialibus, synonymis selectis, locis natalibus, secundum systema sexuale digestas (Impensis Laurentii Salvii). https://doi.org/10.5962/bhl.title.669. https://www.biodiversitylibrary.org/page/358012.

16. Merriam-Webster.com.. Palea. https://www.merriam-webster.com/dictionary/palea.
17. Wang, Y., Bi, X., and Zhong, J. (2022). Revisiting the origin and identity specification of the spikelet: A structural innovation in grasses (Poaceae). Plant Physiol. *190*, 60–71. https://doi.org/10.1093/plphys/kiac257.
18. Soreng, R.J., Peterson, P.M., Romaschenko, K., Davidse, G., Teisher, J.K., Clark, L.G., Barberá, P., Gillespie, L.J., and Zuloaga, F.O. (2017). A worldwide phylogenetic classification of the Poaceae (Gramineae) II: An update and a comparison of two 2015 classifications. J. Syst. Evol. *55*, 259–290. https://doi.org/10.1111/jse.12262.
19. Lombardo, F., and Yoshida, H. (2015). Interpreting lemma and palea homologies: a point of view from rice floral mutants. Front. Plant Sci. *6*, 61. https://doi.org/10.3389/fpls.2015.00061.
20. Xie, P., Wu, Y., and Xie, Q. (2023). Evolution of cereal floral architecture and threshability. Trends Plant Sci. *28*, 1438–1450. https://doi.org/10.1016/j.tplants.2023.08.003.
21. Zong, J., Wang, L., Zhu, L., Bian, L., Zhang, B., Chen, X., Huang, G., Zhang, X., Fan, J., Cao, L., et al. (2022). A rice single cell transcriptomic atlas defines the developmental trajectories of rice floret and inflorescence meristems. New Phytol. *234*, 494–512. https://doi.org/10.1111/nph.18008.
22. Yuan, Z., Gao, S., Xue, D.W., Luo, D., Li, L.T., Ding, S.Y., Yao, X., Wilson, Z.A., Qian, Q., and Zhang, D.B. (2009). RETARDED PALEA1 Controls Palea Development and Floral Zygomorphy in Rice. Plant Physiol. *149*, 235–244. https://doi.org/10.1104/pp.108.128231.
23. Hong, L., DuMond, M., Zhu, M., Tsugawa, S., Li, C.B., Boudaoud, A., Hamant, O., and Roeder, A.H.K. (2018). Heterogeneity and Robustness in Plant Morphogenesis: From Cells to Organs. Annu. Rev. Plant Biol. *69*, 469–495. https://doi.org/10.1146/annurev-arplant-042817-040517.
24. Gilmour, D., Rembold, M., and Leptin, M. (2017). From morphogen to morphogenesis and back. Nature *541*, 311–320. https://doi.org/10.1038/nature21348.
25. Scheres, B. (2001). Plant Cell Identity. The Role of Position and Lineage. Plant Physiol. *125*, 112–114. https://doi.org/10.1104/pp.125.1.112.
26. Kerszberg, M., and Wolpert, L. (2007). Specifying Positional Information in the Embryo: Looking Beyond Morphogens. Cell *130*, 205–209. https://doi.org/10.1016/j.cell.2007.06.038.
27. Coen, E., and Cosgrove, D.J. (2023). The mechanics of plant morphogenesis. Science *379*, eade8055. https://doi.org/10.1126/science.ade8055.
28. Whitewoods, C.D., Gonçalves, B., Cheng, J., Cui, M., Kennaway, R., Lee, K., Bushell, C., Yu, M., Piao, C., and Coen, E. (2020). Evolution of carnivorous traps from planar leaves through simple shifts in gene expression. Science *367*, 91–96. https://doi.org/10.1126/science.aay5433.
29. Meyer, H.M., Teles, J., Formosa-Jordan, P., Refahi, Y., San-Bento, R., Ingram, G., Jönsson, H., Locke, J.C.W., and Roeder, A.H.K. (2017). Fluctuations of the transcription factor ATML1 generate the pattern of giant cells in the Arabidopsis sepal. eLife *6*, e19131. https://doi.org/10.7554/eLife.19131.
30. Roeder, A.H.K., Cunha, A., Ohno, C.K., and Meyerowitz, E.M. (2012). Cell cycle regulates cell type in the Arabidopsis sepal. Development *139*, 4416–4427. https://doi.org/10.1242/dev.082925.
31. Basu, S., Greenwood, J., Jones, A.W., and Nurse, P. (2022). Core control principles of the eukaryotic cell cycle. Nature *607*, 381–386. https://doi.org/10.1038/s41586-022-04798-8.
32. Boudolf, V., Lammens, T., Boruc, J., Van Leene, J., Van Den Daele, H., Maes, S., Van Isterdael, G., Russinova, E., Kondorosi, E., Witters, E., et al. (2009). CDKB1;1 forms a functional complex with CYCA2;3 to suppress endocycle onset. Plant Physiol. *150*, 1482–1493. https://doi.org/10.1104/pp.109.140269.
33. Nowack, M.K., Harashima, H., Dissmeyer, N., Zhao, X., Bouyer, D., Weimer, A.K., De Winter, F., Yang, F., and Schnittger, A. (2012). Genetic framework of cyclin-dependent kinase function in Arabidopsis. Dev. Cell *22*, 1030–1040. https://doi.org/10.1016/j.devcel.2012.02.015.
34. van den Heuvel, S., and Harlow, E. (1993). Distinct Roles for Cyclin-Dependent Kinases in Cell Cycle Control. Science *262*, 2050–2054. https://doi.org/10.1126/science.8266103.
35. Boudolf, V., Barrôco, R., Engler, J.d.A., Verkest, A., Beeckman, T., Naudts, M., Inzé, D., and De Veylder, L. (2004). B1-Type Cyclin-Dependent Kinases Are Essential for the Formation of Stomatal Complexes in Arabidopsis thaliana. Plant Cell *16*, 945–955. https://doi.org/10.1105/tpc.021774.
36. Jiang, S., Wei, J., Li, N., Wang, Z., Zhang, Y., Xu, R., Zhou, L., Huang, X., Wang, L., Guo, S., et al. (2022). The UBP14-CDKB1;1-CDKG2 cascade controls endoreduplication and cell growth in Arabidopsis. Plant Cell *34*, 1308–1325. https://doi.org/10.1093/plcell/koac002.
37. Endo, M., Nakayama, S., Umeda-Hara, C., Ohtsuki, N., Saika, H., Umeda, M., and Toki, S. (2012). CDKB2 is involved in mitosis and DNA damage response in rice. Plant J. *69*, 967–977. https://doi.org/10.1111/j.1365-313X.2011.04847.x.
38. Umeda, M., Umeda-Hara, C., Yamaguchi, M., Hashimoto, J., and Uchimiya, H. (1999). Differential expression of genes for cyclin-dependent protein kinases in rice plants. Plant Physiol. *119*, 31–40. https://doi.org/10.1104/pp.119.1.31.
39. Loog, M., and Morgan, D.O. (2005). Cyclin specificity in the phosphorylation of cyclin-dependent kinase substrates. Nature *434*, 104–108. https://doi.org/10.1038/nature03329.
40. Kumar, N., and Larkin, J.C. (2017). Why do plants need so many cyclin-dependent kinase inhibitors? Plant Signal. Behav. *12*, e1282021. https://doi.org/10.1080/15592324.2017.1282021.
41. Edgar, B.A., Zielke, N., and Gutierrez, C. (2014). Endocycles: a recurrent evolutionary innovation for post-mitotic cell growth. Nat. Rev. Mol. Cell Biol. *15*, 197–210. https://doi.org/10.1038/nrm3756.
42. Qu, X., Yan, M., Zou, J., Jiang, M., Yang, K., and Le, J. (2018). A2-type cyclin is required for the asymmetric entry division in rice stomatal development. J. Exp. Bot. *69*, 3587–3599. https://doi.org/10.1093/jxb/ery158.
43. Ohmori, S., Kimizu, M., Sugita, M., Miyao, A., Hirochika, H., Uchida, E., Nagato, Y., and Yoshida, H. (2009). MOSAIC FLORAL ORGANS1, an AGL6-Like MADS Box Gene, Regulates Floral Organ Identity and Meristem Fate in Rice. Plant Cell *21*, 3008–3025. https://doi.org/10.1105/tpc.109.068742.
44. Li, H., Liang, W., Jia, R., Yin, C., Zong, J., Kong, H., and Zhang, D. (2010). The AGL6-like gene OsMADS6 regulates floral organ and meristem identities in rice. Cell Res. *20*, 299–313. https://doi.org/10.1038/cr.2009.143.
45. Hu, Y., Wang, L., Jia, R., Liang, W., Zhang, X., Xu, J., Chen, X., Lu, D., Chen, M., Luo, Z., et al. (2021). Rice transcription factor MADS32 regulates floral patterning through interactions with multiple floral homeotic genes. J. Exp. Bot. *72*, 2434–2449. https://doi.org/10.1093/jxb/eraa588.
46. Sang, X., Li, Y., Luo, Z., Ren, D., Fang, L., Wang, N., Zhao, F., Ling, Y., Yang, Z., Liu, Y., and He, G. (2012). CHIMERIC FLORAL ORGANS1, Encoding a Monocot-Specific MADS Box Protein, Regulates Floral Organ Identity in Rice. Plant Physiol. *160*, 788–807. https://doi.org/10.1104/pp.112.200980.
47. Reinheimer, R., and Kellogg, E.A. (2009). Evolution of AGL6-like MADS Box Genes in Grasses (Poaceae): Ovule Expression Is Ancient and Palea Expression Is New. Plant Cell *21*, 2591–2605. https://doi.org/10.1105/tpc.109.068239.
48. Ikeda, K., Sunohara, H., and Nagato, Y. (2004). Developmental Course of Inflorescence and Spikelet in Rice. Breed. Sci. *54*, 147–156. https://doi.org/10.1270/jsbbs.54.147.
49. Hu, Y., and Lai, Y. (2015). Identification and expression analysis of rice histone genes. Plant Physiol. Biochem. *86*, 55–65. https://doi.org/10.1016/j.plaphy.2014.11.012.
50. Lee, H.O., Davidson, J.M., and Duronio, R.J. (2009). Endoreplication: polyploidy with purpose. Genes Dev. *23*, 2461–2477. https://doi.org/10.1101/gad.1829209.
51. Ren, D., Rao, Y., Yu, H., Xu, Q., Cui, Y., Xia, S., Yu, X., Liu, H., Hu, H., Xue, D., et al. (2020). MORE FLORET1 Encodes a MYB Transcription Factor

That Regulates Spikelet Development in Rice. Plant Physiol. *184*, 251–265. https://doi.org/10.1104/pp.20.00658.

52. Viola, I.L., Reinheimer, R., Ripoll, R., Manassero, N.G.U., and Gonzalez, D.H. (2012). Determinants of the DNA Binding Specificity of Class I and Class II TCP Transcription Factors. J. Biol. Chem. *287*, 347–356. https://doi.org/10.1074/jbc.M111.256271.
53. Porceddu, A., Stals, H., Reichheld, J.-P., Segers, G., De Veylder, L., Barroco, R.P., Casteels, P., Van Montagu, M., Inzé, D., and Mironov, V. (2001). A Plant-specific Cyclin-dependent Kinase Is Involved in the Control of G2/M Progression in Plants. J. Biol. Chem. *276*, 36354–36360. https://doi.org/10.1074/jbc.M011060200.
54. Lang, L., and Schnittger, A. (2020). Endoreplication — a means to an end in cell growth and stress response. Curr. Opin. Plant Biol. *54*, 85–92. https://doi.org/10.1016/j.pbi.2020.02.006.
55. Schrager-Lavelle, A., Klein, H., Fisher, A., and Bartlett, M. (2017). Grass flowers: An untapped resource for floral evo-devo. J. Syst. Evol. *55*, 525–541. https://doi.org/10.1111/jse.12251.
56. Ciaffi, M., Paolacci, A.R., Tanzarella, O.A., and Porceddu, E. (2011). Molecular aspects of flower development in grasses. Sex. Plant Reprod. *24*, 247–282. https://doi.org/10.1007/s00497-011-0175-y.
57. Hirano, H.Y., Tanaka, W., and Toriba, T. (2014). Grass flower development. Methods Mol. Biol. *1110*, 57–84. https://doi.org/10.1007/978-1-4614-9408-9_3.
58. Wingen, L.U., Münster, T., Faigl, W., Deleu, W., Sommer, H., Saedler, H., and Theißen, G. (2012). Molecular genetic basis of pod corn (Tunicate maize). Proc. Natl. Acad. Sci. USA *109*, 7115–7120. https://doi.org/10.1073/pnas.1111670109.
59. Zhu, M., and Zernicka-Goetz, M. (2020). Principles of Self-Organization of the Mammalian Embryo. Cell *183*, 1467–1478. https://doi.org/10.1016/j.cell.2020.11.003.
60. Sampaio, N.M.V., and Dunlop, M.J. (2020). Functional roles of microbial cell-to-cell heterogeneity and emerging technologies for analysis and control. Curr. Opin. Microbiol. *57*, 87–94. https://doi.org/10.1016/j.mib.2020.08.002.
61. Poursarebani, N., Trautewig, C., Melzer, M., Nussbaumer, T., Lundqvist, U., Rutten, T., Schmutzer, T., Brandt, R., Himmelbach, A., Altschmied, L., et al. (2020). COMPOSITUM 1 contributes to the architectural simplification of barley inflorescence via meristem identity signals. Nat. Commun. *11*, 5138. https://doi.org/10.1038/s41467-020-18890-y.
62. Chai, Y., Liu, H., Chen, W., Guo, C., Chen, H., Cheng, X., Chen, D., Luo, C., Zhou, X., and Huang, C. (2023). Advances in Research on the Regulation of Floral Development by CYC-like Genes. Curr. Issues Mol. Biol. *45*, 2035–2059. https://doi.org/10.3390/cimb45030131.
63. Alvarez-Buylla, E.R., García-Ponce, B., Sánchez, M.P., Espinosa-Soto, C., García-Gómez, M.L., Piñeyro-Nelson, A., and Garay-Arroyo, A. (2019). MADS-box genes underground becoming mainstream: plant root developmental mechanisms. New Phytol. *223*, 1143–1158. https://doi.org/10.1111/nph.15793.
64. Thangavel, G., and Nayar, S. (2018). A Survey of MIKC Type MADS-Box Genes in Non-seed Plants: Algae, Bryophytes, Lycophytes and Ferns. Front. Plant Sci. *9*, 510. https://doi.org/10.3389/fpls.2018.00510.
65. Ito, Y., and Nakano, T. (2015). Development and regulation of pedicel abscission in tomato. Front. Plant Sci. *6*, 442. https://doi.org/10.3389/fpls.2015.00442.
66. Gonzalez, N., Vanhaeren, H., and Inzé, D. (2012). Leaf size control: complex coordination of cell division and expansion. Trends Plant Sci. *17*, 332–340. https://doi.org/10.1016/j.tplants.2012.02.003.
67. Luo, D., Carpenter, R., Vincent, C., Copsey, L., and Coen, E. (1996). Origin of floral asymmetry in Antirrhinum. Nature *383*, 794–799. https://doi.org/10.1038/383794a0.
68. Costa, M.M.R., Fox, S., Hanna, A.I., Baxter, C., and Coen, E. (2005). Evolution of regulatory interactions controlling floral asymmetry. Development *132*, 5093–5101. https://doi.org/10.1242/dev.02085.
69. Kitazawa, M.S. (2021). Developmental stochasticity and variation in floral phyllotaxis. J. Plant Res. *134*, 403–416. https://doi.org/10.1007/s10265-021-01283-7.
70. Ronse De Craene, L. (2016). Meristic changes in flowering plants: How flowers play with numbers. Flora *221*, 22–37. https://doi.org/10.1016/j.flora.2015.08.005.
71. Hiei, Y., Ohta, S., Komari, T., and Kumashiro, T. (1994). Efficient transformation of rice (Oryza sativa L.) mediated by Agrobacterium and sequence analysis of the boundaries of the T-DNA. Plant J. *6*, 271–282. https://doi.org/10.1046/j.1365-313X.1994.6020271.x.
72. Zhang, H., Zhang, J., Wei, P., Zhang, B., Gou, F., Feng, Z., Mao, Y., Yang, L., Zhang, H., Xu, N., and Zhu, J.K. (2014). The CRISPR/Cas9 system produces specific and homozygous targeted gene editing in rice in one generation. Plant Biotechnol. J. *12*, 797–807. https://doi.org/10.1111/pbi.12200.
73. Itoh, J.I., Kitano, H., Matsuoka, M., and Nagato, Y. (2000). Shoot organization genes regulate shoot apical meristem organization and the pattern of leaf primordium initiation in rice. Plant Cell *12*, 2161–2174. https://doi.org/10.1105/tpc.12.11.2161.
74. Li, N., Zhang, D.-S., Liu, H.-S., Yin, C.-S., Li, X.-X., Liang, W.-Q., Yuan, Z., Xu, B., Chu, H.-W., Wang, J., et al. (2006). The rice tapetum degeneration retardation gene is required for tapetum degradation and anther development. Plant Cell *18*, 2999–3014. https://doi.org/10.1105/tpc.106.044107.
75. Wang, F.-X., Shang, G.-D., Wu, L.-Y., Mai, Y.-X., Gao, J., Xu, Z.-G., and Wang, J.-W. (2021). Protocol for assaying chromatin accessibility using ATAC-seq in plants. Star Protoc. *2*, 100289. https://doi.org/10.1016/j.xpro.2020.100289.
76. Kouchi, H., and Hata, S. (1993). Isolation and characterization of novel nodulin cDNAs representing genes expressed at early stages of soybean nodule development. Mol. Gen. Genet. *238*, 106–119. https://doi.org/10.1007/BF00279537.
77. Tao, J., Liang, W., An, G., and Zhang, D. (2018). OsMADS6 Controls Flower Development by Activating Rice FACTOR OF DNA METHYLATION LIKE1. Plant Physiol. *177*, 713–727. https://doi.org/10.1104/pp.18.00017.
78. Zhu, W., Yang, L., Wu, D., Meng, Q., Deng, X., Huang, G., Zhang, J., Chen, X., Ferrándiz, C., Liang, W., et al. (2022). Rice SEPALLATA genes OsMADS5 and OsMADS34 cooperate to limit inflorescence branching by repressing the TERMINAL FLOWER1-like gene RCN4. Plant Cell *233*, 1682–1700. https://doi.org/10.1111/nph.17855.
79. Bowler, C., Benvenuto, G., Laflamme, P., Molino, D., Probst, A.V., Tariq, M., and Paszkowski, J. (2004). Chromatin techniques for plant cells. Plant J. *39*, 776–789. https://doi.org/10.1111/j.1365-313X.2004.02169.x.
80. Li, G., Liang, W., Zhang, X., Ren, H., Hu, J., Bennett, M.J., and Zhang, D. (2014). Rice actin-binding protein RMD is a key link in the auxin-actin regulatory loop that controls cell growth. Proc. Natl. Acad. Sci. USA *111*, 10377–10382. https://doi.org/10.1073/pnas.1401680111.
81. Yuan, Y., Xu, H., and Leung, R.K. (2016). An optimized protocol for generation and analysis of Ion Proton sequencing reads for RNA-Seq. BMC Genomics *17*, 403. https://doi.org/10.1186/s12864-016-2745-8.
82. Wang, D., Li, J., Sun, L., Hu, Y., Yu, J., Wang, C., Zhang, F., Hou, H., Liang, W., and Zhang, D. (2021). Two rice MYB transcription factors maintain male fertility in response to photoperiod by modulating sugar partitioning. New Phytol. *231*, 1612–1629. https://doi.org/10.1111/nph.17512.

STAR★METHODS

KEY RESOURCES TABLE

REAGENT or RESOURCE	SOURCE	IDENTIFIER
Antibodies		
Rabbit Polyclonal Anti-OsMADS6	ABclonal	Customer order
Rabbit Polyclonal Anti-OsMADS32	ABclonal	Customer order
Goat Anti-Rabbit IgG-HRP	Bio-Rad	CAT#: STAR121; RRID: AB_567026
Goat Anti-Mouse IgG-HRP	Proteintech	CAT#: SA00001-2; RRID: AB_2722564
Anti-Digoxigenin-AP, Fab Fragments	Roche	CAT#: 11093274910; RRID: AB_514497
Anti-HA Antibody	Abmart	CAT#: M20003M; RRID: AB_2864345
Bacterial and virus strains		
Escherichia coli DH5α	WEIDI	CAT#: DL1001
Agrobacterium EHA105	WEIDI	CAT#: AC1010
Agrobacterium GV3101	WEIDI	CAT#: AC1001
Chemicals, peptides, and recombinant proteins		
Hygromycin B	Solarbio	CAT#: H8080
Toluidine blue	Sangon Biotech	CAT#: E670105
Trizol	Invitrogen	CAT#: 15596018
Histo-Clear II	National Diagnotics	CAT#: HS-202
Bovine serum albumin (BSA), 30%	Sigma	CAT#: A7284
Protease inhibitor cocktail	Roche	CAT#: 4693116001
4',6-diamidino-2-phenylindole (DAPI)	Sigma	CAT#: 32670
NBT/BCIP stock	Roche	CAT#: 11681451001
Bradford reagent	bioknow	CAT#: C503041-1000
Critical commercial assays		
In-Fusion HD Cloning Kit	Takara	CAT#: 639648
FastQuant RT Kit with gDNase	Tiangen	CAT#: KR106
QuantiNova SYBR Green PCR Kit	QIAGEN	CAT#: 208052
DIG RNA Labelling Kit	Roche	CAT#: 11175025910
Dual-Luciferase reporter kit	Promega	CAT#: E1980
TNT T7/SP6 Coupled Wheat Germ Extract System	Promega	CAT#: L5030
RNAeasy kit	Qiagen	CAT#: 74004
Chemiluminescent Nucleic Acid Detection Module	Thermo	CAT#: 89880
Deposited data		
RNA-sequencing data	This paper	GEO: GSE260950
Experimental models: Organisms/strains		
Rice: *rep1-1*	Yuan et al.[22]	N/A
Rice: *Osmads6-2*	Ohmori et al.[43]	N/A
Rice: *Osmads32-2*	Hu et al.[45]	N/A
Rice: *Osmads6-2 rep1-1*	This paper	N/A
Rice: *Osmads6-2* (+/-) *rep1-1*	This paper	N/A
Rice: *Osmads6-2 rep1-1* (+/-)	This paper	N/A
Rice: *Osmads32-2 Osmads6-2*	This paper	N/A
Rice: Osmads32-2 *rep1-1*	This paper	N/A
Rice: *Osmads32-2 Osmads6-2 rep1-1*	This paper	N/A
Rice: $REP1_{pro}$::$OsMADS6_{gDNA}$/*Osmads6*	This paper	N/A
Rice: $OsMADS6_{pro}$::$REP1_{gDNA}$ /*rep1*	This paper	N/A
Rice: *OsCDKB2;1D-N/Osmads6-2*	This paper	N/A

(*Continued on next page*)

Continued

REAGENT or RESOURCE	SOURCE	IDENTIFIER
Rice: *OsCDKB2;1D-N*/WT	This paper	N/A
Rice: *OsCDKB2;1-CRISPR*/WT	This paper	N/A
Rice: *OsCDKB1;1*/WT	This paper	N/A
Rice: *OsCDKB1;1/rep1-1*	This paper	N/A
Arabidopsis: *35S::MADS6*	This paper	N/A
Arabidopsis: *35S::MADS32*	This paper	N/A
Arabidopsis: *35S::REP1*	This paper	N/A
Oligonucleotides		
Primers used in this study, see Table S3	This paper	N/A
Recombinant DNA		
$REP1_{pro}$::$OsMADS6_{gDNA}$	This paper	N/A
$OsMADS6_{pro}$::$REP1_{gDNA}$	This paper	N/A
OX-OsCDKB2;1D-N	This paper	N/A
OX-OsCDKB1;1	This paper	N/A
OsCDKB2;1-CRISPR	This paper	N/A
35S::MADS6	This paper	N/A
35S::MADS32	This paper	N/A
35S::REP1	This paper	N/A
PGreen0000-MADS6	This paper	N/A
PGreen0000-MADS32	This paper	N/A
PGreen0000-REP1	This paper	N/A
pOsMADS6::LUC	This paper	N/A
pREP1::LUC	This paper	N/A
pOsCDKB1;1::LUC	This paper	N/A
pOsCDKB2;1::LUC	This paper	N/A
Software and algorithms		
ImageJ	National Institutes of Health	https://imagej.net/software/imagej/
SPSS statistics version 25	International Business Machines Corporation	https://www.ibm.com/support/pages/ibm-spss-statistics250x
Summit 5.2	Beckman Coulter	https://www.beckman.com/flow-cytometry/software
GraphPad Prism	GraphPad Software	https://www.graphpad-prism.cn/
FlowJo V10	BD Biosciences	https://www.bdbiosciences.com/en-us/products/software/flowjo-v10-software
The Rice genome	The Rice Annotation Project	https://rapdb.dna.affrc.go.jp/
China Rice Data Center	China National Rice Research Institute	https://www.ricedata.cn/
KEGG database	International Business Machines Corporation	https://www.genome.jp/kegg/

RESOURCE AVAILABILITY

Lead contact

Further information and requests for resources and reagents should be directed to and will be fulfilled by the Lead Contact, Zheng Yuan (zyuan@sjtu.edu.cn).

Materials availability

Plasmids and other reagents generated in this study will be available upon request from the lead contact with a completed Materials Transfer Agreement.

Data and code availability

- RNA-seq data have been deposited at GEO and are publicly available as of the date of publication. Accession numbers are listed in the key resources table.
- This paper does not report original code.
- Any additional information required to reanalyze the data reported in this paper is available from the lead contact upon request.

EXPERIMENTAL MODEL AND STUDY PARTICIPANT DETAILS

Plant materials and growth conditions

The mutants *rep1-1* was in 9522 genetic backgrounds (wild type, *O. sativa L. ssp. japonica*); *Osmads6-2* was a *Tos17* retrotransposon insertion mutant in *Nipponbare* background.[44] *Osmads32-2* (named *mfo1-2* in previous study), was a T-DNA insertion mutant in AF36 background.[45] Double and triple mutants were isolated by phenotype observation and confirmed by genotyping. All rice plants were grown in the paddy field of Shanghai Jiao Tong University, located in Shanghai (31.03°N, 121.45°E). Arabidopsis seeds were sterilized with 70% ethanol and germinated on 1/2 Murashige and Skoog medium (pH 5.8). Plants were grown at 21°C under a 15h light/9h dark cycle.

METHOD DETAILS

Constructs and plant transformation

The transformation of plasmids was introduced to the rice callus by the *Agrobacterium*-mediated method using hygromycin B for selection. Callus was cultured from the sheared young inflorescences at 28°C under dark conditions for 12 to 15 d.[71]

To construct overexpression vector for *OsCDKB1;1*, the full-length cDNA generated with primers OX-CDKB1;1-F/R was cloned into vector *PTCK303* driven by the *Ubiquitin* promoter using In-Fusion HD Cloning Kit (Takara, Cat No./ID: 639648). For *OsCDKB2;1D-N* overexpression, the overlapping cDNAs carrying the mutations were amplified with primers OX-CDKB2;1D-N(P1)-F/R and OX-CDKB2;1D-N(P2)-F/R as previously described and cloned into the overexpression vector *PTCK303*.[34] Primers used for constructing *OX-CDKB1;1*, *OX-OsCDKB2;1D-N* are listed in Table S3. The *OX-CDKB1;1* construct was transferred into WT and *rep1-1* mutant callus respectively. The *OsCDKB2;1D-N* plasmid was transferred into WT and *Osmads6-2* mutant backgrounds respectively.

The *CRISPR-OsCDKB2;1* knockout mutant was obtained using CRISPR/Cas9 technology as described previously by Zhang et al.[72] Primers used for constructing dual guide RNA (CDKB2;1sgRNA) are listed in Table S3. Plant genotyping was performed by PCR amplification of the mutation-bearing regions, followed by the sequencing of the resultant PCR products. The primers used for PCR are listed in Table S3.

The primers *OsM6* pro-F/R were used to amplify the 3177-bp sequence of the *OsMADS6* promoter and cloned into the ECORI and BamHI sites of *pCAMBIA1301* vector, thus replacing the *CaMV 35S* promoter to generate *pCAMBIA1301-proOsMADS6*. The 1221-bp *REP1* genomic sequence (containing a 729-bp coding region and a 492-bp fragment downstream of TGA) was amplified from WT using the primers *REP1* gDNA-1F/R and cloned into BamHI and SalI sites of *pCAMBIA1301-proOsMADS6* vector to generate the $OsMADS6_{pro}::REP1_{gDNA}$ plasmid. The constructed $OsMADS6_{pro}::REP1_{gDNA}$ vector was introduced into WT and *rep1-1* mutant calli respectively. The 3288-bp *REP1* promoter sequence was amplified from WT using the primers REP1 pro-F/R and cloned into the p*CAMBIA1301* vector to generate the *pCAMBIA1301-proREP1* plasmid. The 7967-bp *OsMADS6* genomic sequence was amplified from WT using the primers OsM6 gDNA-1F/R and cloned into *pCAMBIA1301-proREP1* vector to generate the $REP1_{pro}::OsMADS6_{gDNA}$ plasmid. The constructed $REP1_{pro}::OsMADS6_{gDNA}$ vector was introduced into WT and *Osmads6-2* mutant calli respectively.

The full-length cDNA of *OsMADS6*, *OsMADS32* and *REP1* generated with primers PHB-OsM32-F/R, PHB-OsM6-F/R and PHB-REP1-F/R, respectively, and cloned into the *PHB* vector under control of the *35S* promoter using the In-Fusion HD Cloning Kit (Takara, Cat No./ID: 639648). The overexpression constructs were transferred into Col-0 plants by *Agrobacterium*-mediated transformation using the floral dip method.[36] All transgenic lines were selected on medium supplemented with 30-50 μg/ml hygromycin.

Histological analysis and microscopy observation

To measure the width and length of the palea, spikelets were collected along the inflorescence axis, fixed in FAA (10% formalin, 50% ethanol, and 5% acetic acid) and dehydrated in a series of graded ethanol.[73] Specimens were critical point dried with CO_2, mounted on stubs, sputter-coated with gold, and observed under a JSM-6360LV scanning electron microscope (JEOL, Tokyo, Japan). To ensure consistent measurement in palea development analysis, we defined the palea width at its widest point and the length along the proximodistal axis. The spikelets in rice inflorescences develop in order, and the maximum width and length of the palea within a given inflorescence are correlated (Figure S1A). For convenient sampling, we observed the entire inflorescence before Pa-es 3, and monitored the growth of the paleas throughout their entire growth cycle, from the third and the fourth spikelet below the terminal spikelet on the main inflorescence axis after Pa-es 3. To quantify the shape and number of the epidermal cells in the palea, SEM continuous image stacks along proximodistal axis and mediolateral axes of MRP and BOP were captured. The epidermis of MRP and BOP was divided into nine areas based on the length and width of the palea (Figure S1C). Characteristics and measurements

for palea staging analysis were obtained from the intermediate epidermal region using ImageJ. The count of epidermal cells in the palea was determined within nine epidermal regions using ImageJ. Analysis included the number of cells per unit area, epidermal cell number, and longitudinal (along the proximal-distal axis) and transverse (along the lemma-palea axis) cell length. For early stages of palea primordia (~Pa-es 5), dehydrated lemma was dissected with precision tweezer under Stereoscopic microscope (Leica, Wetzlar, Germany).

Rice mature spikelets, Arabidopsis leaf and floral tissues at different developmental stages fixed in FAA, were dissected as necessary to identify internal floral organs, and then dehydrated in an alcohol series. For histological analysis, tissues were embedded in resin. Materials were sectioned to 8 mm thick and stained with toluidine blue (Bio Basic, CAT#: E670105) and photographed using a Nikon E600 microscope and a Nikon DXM1200 digital camera.[74] The methods for statistical analysis and morphological observation are the same as above.

Flow cytometry analysis

For flow cytometry, rice spikelets, split MRP, BOP or Arabidopsis seedlings were chopped with a razor blade in 1.5 mL Modified G buffer (45 mM $MgCl_2$, 20 mM MOPS, 30 mM sodium citrate, 1% PVP-40, 0.2% TritonX-100, 10 mM Na_2EDTA, 20 μl/ml β-Mercaptoethanol, pH 7.0). In WT nuclear ploidy analysis, the entire spikelets were collected from inflorescences that were less than 1cm in length, which posed a challenge in manually removing the palea MRP from BOP. When the inflorescence exceeded 1cm, analysis was performed on split MRP, BOP, and whole spikelets. For nuclear ploidy analysis of *Osmads6-2* and *rep1-1* mutants, the whole spikelets from inflorescences were collected because they exhibited a relatively comparable nature to WT spikelets. The nuclei were filtered through a 30-μm mesh and stained with 10 μM DAPI staining solution. The nuclear DNA content was analyzed with a flow cytometer (BD biosciences, FACSAria II).[75]

Quantitative reverse-transcription PCR assays

Total RNA from three biological replicates was extracted from rice organs using Trizol reagent (Invitrogen, Cat No./ID: 15596018). The RNA sample was reverse transcribed into cDNA using FastQuant RT Kit with gDNase (Tiangen, Cat No./ID: KR106). RT-qPCR was performed in triplicate using the LightCycler 96 Real-Time PCR System (Roche) with QuantiNova SYBR Green PCR Kit (QIAGEN, Cat No./ID: 208052) using primers as described in Table S3. The *OsACTIN* gene (LOC_Os03g50885) and *AtACT2* (AT3G18780) were used to normalize expression levels.

In situ hybridization

Fresh rice inflorescences and florets (Phase A-C) were harvested and immediately fixed in FAA solution, dehydrated, infiltrated, and embedded in paraffin as described previously in "Histological analysis and microscopy observation". Probes were labeled with digoxigenin using the DIG RNA Labelling Kit (Roche, Cat No./ID: 11175025910) and primers were listed in Table S3. The samples were sectioned into 6-8 μm thin using a clean microtome. These slices were subsequently placed on suitable glass slides and subjected to tissue hydration using an ethanol series. DIG-labeled RNA probe was diluted in the proper hybridization mix (50% formamide, 300 mM NaCl, 10 mM Tris-HCl pH 7.5, 1 mM EDTA, 1x Denharts, 10% dextransulphate, 10 mM DTT, 250 ng/ml tRNA, 100 μg/ml poly(A); count 200 μl/slide of hybridization mix, 3 μl/slide of DIG-RNA probe). Subsequently, the slides were covered with a coverslip, positioned in a humidified box with 50% formamide/2x SSC, and hybridized overnight at 45°C. Formamide washing was performed as described by Kouchi and Hata.[76] Each slide was incubated with proper dilution Anti-DIG antibody (-Digoxigenin-AP, Fab fragments, Roche, Cat No./ID: 11093274910, diluted at 1:10000 for *OsMADS6* and *HISTONE4*, diluted at 1:1000 for *OsCDKB2;1* and *OsCDKB1;1*, diluted at 1:500 for *REP1*) in buffer (0.5%BSA, 0.3% Triton X 100, 100mM Tris HCl pH 7.5, 150mM NaCl) for 2h in a humidified box. For color reaction, each slide was incubated with NBT/BCIP (NBT/BCIP stock, Roche, Cat No./ID: 11681451001, diluted at 1:50) in buffer (100mM Tris-HCl pH 9.5, 100mM NaCl, 50mM $MgCl_2$) overnight in a dark humidified box. Images were obtained using a Nikon Eclipse 80i microscope.

Dual-luciferase assay

The dual-luciferase (LUC) transactivation assay was performed in *Nicotiana benthamiana* leaves leaves.[77] The full length cDNAs of *OsMADS6*, *OsMADS32* and *REP1* were cloned into *pGreenII-0000*. The empty vector *pGreenII-0000* was used as the negative control. The reporter *pOsMADS6::LUC*, *pREP1::LUC*, *pOsCDKB1;1::LUC*, *pOsCDKB2;1::LUC* were constructed by cloning the gene promoter sequence upstream of the start codon into the vector *pGreenII-0800-LUC* to drive *LUC* expression. Primers used are available in Table S3. The transformations of effectors and reporters were introduced into *Agrobacterium tumefaciens* GV3101 and infiltrated into 4-week-old *N. benthamiana* leaves.[78] Each sample was with six biological replicates. The LUC/REN activities ratio was measured using the Dual-Luciferase reporter kit (Promega, Cat No./ID: E1980) in a GloMax 20/20 luminometer (Promega).

ChIP-qPCR

The ChIP assay method was modified from the protocol described by Bowler et al.[79] Approximately 1 g of WT rice inflorescence < 1 cm in length was crosslinked in extraction buffer (1% (v/v) formaldehyde, 0.4 M sucrose, 10 mM Tris-HCl, 5 mM β-mercaptoethanol, 0.1 mM PMSF and protease inhibitor cocktail, pH 8.0) and sonicated to yield chromatin DNA with a length of 200 to 500 bp. Chromatin protein concentration was measured using a Bradford reagent (Bioknow, Cat No./ID: C503041-1000). The sonicated chromatin DNA samples (200- 400 μg amounts) were used for immunoprecipitation, and 10% nonsonicated chromatin

DNA was reverse cross-linked and served as the total input DNA control. Immunoprecipitation was performed using an OsMADS6- or OsMADS32- specific antibody bound to Dynabeads Protein G for Immunoprecipitation (Invitrogen, Cat No./ID: 10003D). The immunoprecipitated proteins and DNA were eluted with 1% (w/v) SDS, 0.1 M $NaHCO_3$ and 200 mM NaCl, and the crosslink was reversed by incubation at 65 °C, 600rpm overnight. The precipitated and recovered *REP1* and *OsCDKB2;1* promoter fragments were quantified by RT-qPCR using primers listed in Table S3, and the relative quantification of enrichment was normalized by input DNA sample.[80] All those primer pairs that were repeated at least three times.

Electrophoretic mobility-shift (EMSA) assays

The EMSA method was modified from the protocol described by Zhu et al.[78] The full-length cDNAs of *OsMADS6* and *REP1* were cloned into *pGADT7* vector and used the TNT T7/SP6 Coupled Wheat Germ Extract System (Promega, Cat No./ID: L5030) for in vitro transcription and translation. The protein concentration was determined using a Bradford reagent (Bioknow, Cat No./ID: C503041-1000). The protein samples (10 μg amounts) were electrophoresed in 10% SDS-PAGE and the gels were transferred to nitrocellulose membranes. The membranes were blocked with PBS buffer (1.3M NaCl, 70mM Na_2HPO_4, 30mM NaH_2PO_4, pH7.0) supplemented with 5% non-fat milk overnight at 4 °C, and incubated with primary antibodies (Anti-HA antibody, Abmart, Cat No./ID: M20003M, diluted at 1:3000) in PBS buffer with 5% non-fat milk for 2 h. Afterwards, the membranes were washed three times (10 min each) with PBS buffer and incubated with the secondary antibodies (Goat Anti-Mouse IgG H&L (HRP), bioknow, Cat No./ID: SA00001-2, dilution at 1:3000) for 2 h. After washing three times with PBS buffer, the membranes were incubated with a chromogenic agent using the Chemiluminescent Nucleic Acid Detection Module (Thermo, Cat No./ID: 89880). Annealed two complementary primers containing or without FAM at the 5'-end to generate fluorescein amidite (FAM)-labeled probes or nonlabelled probes. The binding reaction mixture contained 25 mM Tris-acetate (pH 7.5), 1 mM DTT, 0.1 mg/ml BSA, 2 mM MgAc, 20 nM FAM-labelled DNA, and 3 μl of in vitro synthesized protein (10 μg amounts). The concentrations of OsMADS6 and REP1 proteins were approximately 2.8 mg/ml and 3.5 mg/ml, respectively. The binding reaction was performed for 30 min at 25°C before loading on a 6% native polyacrylamide gel. Competition was tested using 50-fold excess of nonlabelled probes. FAM-labelled probes were visualized using the FAM channel of a ChemiDoc MP imaging system (BioRad, Hercules, CA, USA). Primers are listed in Table S3.

RNA-Sequencing (RNA-Seq) and analysis

RNA-seq libraries were generated from 2-5 μg total RNA (RNAeasy kit, Qiagen, Cat No./ID: 74004) and enriched with Dynabeads mRNA Purification Kit (Thermo Fisher, Cat No./ID: 61006) using methods described by Yuan et al.[81] Libraries were size-selected for read length up to 300 bp using Ion Torrent Proton (Thermo Fisher) for single-end sequencing. Libraries were quantified on an Agilent bioanalyzer (Agilent) and Mapsplice was used for RNA-seq alignment. The data were normalized using the Upper-quartile normalization method, and the algorithm DESeq was used to identify differentially expressed genes (DEGs). The obtained P-values were calculated using the Benjamini-Hochberg false discovery rate (BH-FDR) algorithm.[45] Genes were considered to be significantly differentially expressed if the FDR < 0.05, P-value < 0.05 and the fold change > 2.0. Fisher's test was used to identify relevant gene ontology (GO) pathways, and the threshold of significance was defined by P-value.[82] Pathways in which DEGs are involved were identified based on the KEGG database.

Accession numbers

Locus identifications in the Rice Genome Annotation Project Database are as follows: *REP1* (Os09g24480), *OsMADS6* (Os02g45770), *OsMADS32* (Os01g52680), *OsCDKB1;1* (Os01g0897000), *OsCDKB2;1* (Os08g0512600). *OsMYB63* (Os04g50770), *OsMYB-like* (Os06g24070), *CCT/B-box Zinc Finger* (Os06g44450), *AP2-like1* (Os03g08490), *OsWRKY76* (Os09g25060), *TF-X1* (Os01g03570). Accession numbers for the differentially expresses genes used in the phylogenetic analysis are as follows: *OsCycA2;1* (Os12g0502300), *OsCycB1;1* (Os01g0805600), *OsCycB2;1* (Os04g47580), *OsCycB2;2* (Os06g0726800), *OsCycD3;1* (Os06g0217900), *OsCycD4;1* (Os09g29100), *OsCycD4;2* (Os08g37390), *OsCycD6;1* (Os07g37010), *OsCycD5;3* (Os03g0203800), *OsCycD2;1* (Os07g0620800), *OsCycD1;3* (Os08g32540), *OsCycD5;2* (Os12g0588800), *OsCycD1;1* (Os06g0236600), *OsDEL2* (Os06g13670), *OsKRP1* (Os02g0762400), *OsKRP3* (Os11g0614800), *OsWee1* (Os02g0632100), *OsSDS* (Os03g0225200), *OsKRP5* (Os09g0459900).

QUANTIFICATION AND STATISTICAL ANALYSIS

Statistical analysis

All detailed statistical details parameters of the experiments can be found in the figure legends, including the type of statistical tests used, the exact value of n, and what n represents. The Statistical works were run with SPSS Statistics 25 (IBM). All data were shown as means ± SD. Statistical significance level of $P < 0.05$ between different sample groups was tested using ANOVA.